The current issue and full text archive of this journal is available at
www.emeraldinsight.com/0961-5539.htm

A finite element model of the squeeze casting process

Roland W. Lewis, Eligiusz W. Postek, Zhiqiang Han and David T. Gethin
School of Engineering, University of Wales Swansea, Swansea, UK

Received December 2004
Revised September 2005
Accepted November 2005

Abstract

Purpose – To present a numerical model of squeeze casting process.

Design/methodology/approach – The modelling consists of two parts, namely, the mould filling and the subsequent thermal stress analysis during and after solidification. Mould filling is described by the Navier-Stokes equations discretized using the Galerkin finite element method. The free surface is followed using a front tracking procedure. A thermal stress analysis is carried out, assuming that a coupling exists between the thermal problem and the mechanical one. The mechanical problem is described as an elasto-visco-plastic formulation in an updated Lagrangian frame. A microstructural solidification model is also incorporated for the mould filling and thermal stress analysis. The thermal problem is solved using enthalpy method.

Findings – During the mould-filling process a quasi-static arbitrary Lagrangian-Eulerian (ALE) approach and a microstructural solidification model were found to be applicable. For the case of the thermal stress analysis the influence of gap closure, effect of initial stresses (geometric nonlinearity), large voids and good performance of a microstructural model have been demonstrated.

Research limitations/implications – The model can also be applied to the simulation of indirect castings. The final goal of the model is the ability to simulate the forming of the material after mould filling and during the solidification of the material. This is possible to achieve by applying arbitrary contact surfaces due to the sliding movement of the cast versus the punch and die.

Practical implications – The presented model can be used in engineering practice, as it incorporates selected second-order effects which may influence the performance of the cast.

Originality/value – During the mould-filling procedure a quasi-static ALE approach has been applied to SQC processes and found to be generally applicable. A microstructural solidification model was applied which has been used for the thermal stress analysis only. During the thermal stress analysis the influence of gap closure and initial stresses (geometric nonlinearity) has been demonstrated.

Keywords Couplers, Thermo-mechanical separation, Fluid dynamics, Solidification, Modelling, Finite element analysis

Paper type Research paper

1. Introduction

The paper deals with the presentation of a squeeze casting model which is currently being developed. The problem consists of two parts, namely, a mould filling simulation and a thermal stress analysis. Common problems between the two stages involve the thermal problem and solidification. The Navier-Stokes equations are used to describe the flow problem and are solved by using the Galerkin finite element method. The free surface tracking problem has been solved using a pseudo-concentration function method. The advection equation is discretized using the Taylor-Galerkin

The authors would like to thank the Engineering and Physical Sciences Research Council (UK) Grant No. GR/R80001/01 and GKN Squeezeform for their support.

International Journal of Numerical Methods for Heat & Fluid Flow
Vol. 16 No. 5, 2006
pp. 539-572

0961-5539
DOI 10.1108/09615530610669102

method. During the solution of the thermal problem the enthalpy method was applied. The thermomechanical problem has been treated as coupled and solved using a staggered approach. Finally, some applications of a microstructural solidification model have been presented. The microstructural model was used during the mould filling and thermal stress analysis stages. The application of microstructural solidification models allow us to better predict the material properties and in effect the residual stress distribution. Some other aspects of concern, e.g. the influence of second order effects such as initial stresses, voids, etc. have also been investigated. A comprehensive overview of the squeeze casting process has been presented by Ghomashchi and Vikhrov (2000). A description of thermomechanical problems has also been given by Sluzalec (1992), Vaz and Owen (1996) and Kleiber (1993). The Galerkin and Taylor-Galerkin methods have been described in detail by Taylor and Hughes (1981), Zienkiewicz and Taylor (2000) and Donea and Huerta (2003). Methods of solving such thermal problems, including phase transformation, are described by Lewis *et al.* (1996) and Celentano (1994).

2. Thermal problem

2.1 Problem formulation

Let us consider the heat transfer equation of the form:

$$\nabla(k\nabla T) + q = \rho c_p \frac{\partial T}{\partial t} \quad \text{on} \quad \Omega \tag{1}$$

where k is the thermal conductivity, ∇T is the temperature gradient, q is the heat source, ρ is the mass density and c_p is the heat capacity. The equation is determined over the body Ω and fulfils the following Dirichlet and Neumann boundary conditions, respectively:

$$S_1(T) = T - T_w = 0 \ \text{ on } \ \partial\Omega_1 \quad S_2(T) = k\left(\frac{\partial T}{\partial n}\right) + h(T - T_w) \ \text{ on } \ \partial\Omega_2 \tag{2}$$

where T_w is the temperature of the wall and $\partial T/\partial n$ is the heat flux normal to the boundary $\partial\Omega_2$. On applying the weighted residual method to equations (1) and (2) in the form:

$$\int_{\Omega} wF \, \mathrm{d}\Omega = 0 \tag{3}$$

we obtain:

$$\int_{\Omega} w\left(\nabla(k\nabla T) + q - \rho c_p \frac{\partial T}{\partial t}\right)\mathrm{d}\Omega = 0, \quad \int_{\Omega} w\left(\nabla(k\nabla T) + q - \rho c_p \frac{\partial T}{\partial t}\right)\mathrm{d}\Omega = 0, \tag{4}$$

and eventually we arrive at:

$$\int_{\Omega} w\left(\nabla(k\nabla T) + q - \rho c_p \frac{\partial T}{\partial t}\right)\mathrm{d}\Omega + \sum_{i=1}^{2} \int_{\partial\Omega_i} w_i S_i \mathrm{d}(\partial\Omega_i) = 0 \tag{5}$$

Integrating equation (5) and making use of Green's theorem we obtain:

$$\int_{\Omega} \nabla w(k\nabla T)\mathrm{d}\Omega - \int_{\Omega} wq\,\mathrm{d}\Omega - \int_{\Omega} w\rho c_p \frac{\partial T}{\partial t}\mathrm{d}\Omega - \int_{\partial\Omega_1} w_1 k \frac{\partial T}{\partial n}\mathrm{d}(\partial\Omega) - \int_{\partial\Omega_2} w_2\left(k\frac{\partial T}{\partial n} + h(T - T_w)\right)\mathrm{d}(\partial\Omega) = 0 \tag{6}$$

Since, the weighting functions, w_i, are arbitrary we may choose a set of the functions such that $w_2 = w_1 = -w$ which yields the following "weak" form of the problem, i.e.

$$\int_{\Omega} \nabla w k \nabla T\,\mathrm{d}\Omega - \int_{\Omega} wq\,\mathrm{d}\Omega - \int_{\Omega} w\rho c_p \frac{\partial T}{\partial t}\mathrm{d}\Omega + \int_{\partial\Omega_2} wh(T - T_w)\mathrm{d}(\partial\Omega) - \int_{\partial\Omega_1} wk\frac{\partial T}{\partial n}\mathrm{d}(\partial\Omega) = 0 \tag{7}$$

Assuming the approximation of the temperature field to be of the form $\mathbf{T} = \mathbf{N}\mathbf{T}_\mathbf{N}$, where $\mathbf{N}$ is the shape function matrix and $\mathbf{T}_\mathbf{N}$ is the vector of nodal temperatures and setting $w_i = N_i$ (i.e. using the Galerkin method) we obtain the discretized form of equation (7), i.e.

$$\mathbf{K}\mathbf{T}_N + \mathbf{C}\dot{\mathbf{T}}_N = \dot{\mathbf{F}} \tag{8}$$

where $\mathbf{K}$ and $\mathbf{C}$ are the conductivity and heat capacity matrices, respectively, and $\mathbf{F}$ is the thermal loading vector, i.e.

$$K_{ij} = \int_{\Omega} \nabla N_i k \nabla N_j \mathrm{d}\Omega + \int_{\partial\Omega_3} N_i h N_j \mathrm{d}(\partial\Omega) - \int_{\partial\Omega_1} N_i k \frac{\partial N_j}{\partial n}\mathrm{d}(\partial\Omega)$$
$$C_{ij} = \int_{\Omega} N_i c_p \rho N_j\,\mathrm{d}\Omega, \quad F_i = \int_{\Omega} N_i q\,\mathrm{d}\Omega + \int_{\partial\Omega_3} N_i h T_w \mathrm{d}(\partial\Omega) \tag{9}$$

Equation (9) can be solved using either implicit or explicit time marching schemes. In the case of the mould filling analysis an explicit scheme was chosen while during the thermal stress analysis an implicit integration rule was utilised, namely the Crank-Nicholson scheme.

2.2 Enthalpy method

For the case of phase transformation, due to the existence of a strong discontinuity in the dependence of heat capacity with respect to time, Figure 1(a), the enthalpy method has been applied, as shown by Lewis *et al.* (1978, 1996). The essence of the enthalpy method is the involvement of a new variable (enthalpy). This allows us to regularize the sharp change in heat capacity, due to latent heat release, during the phase

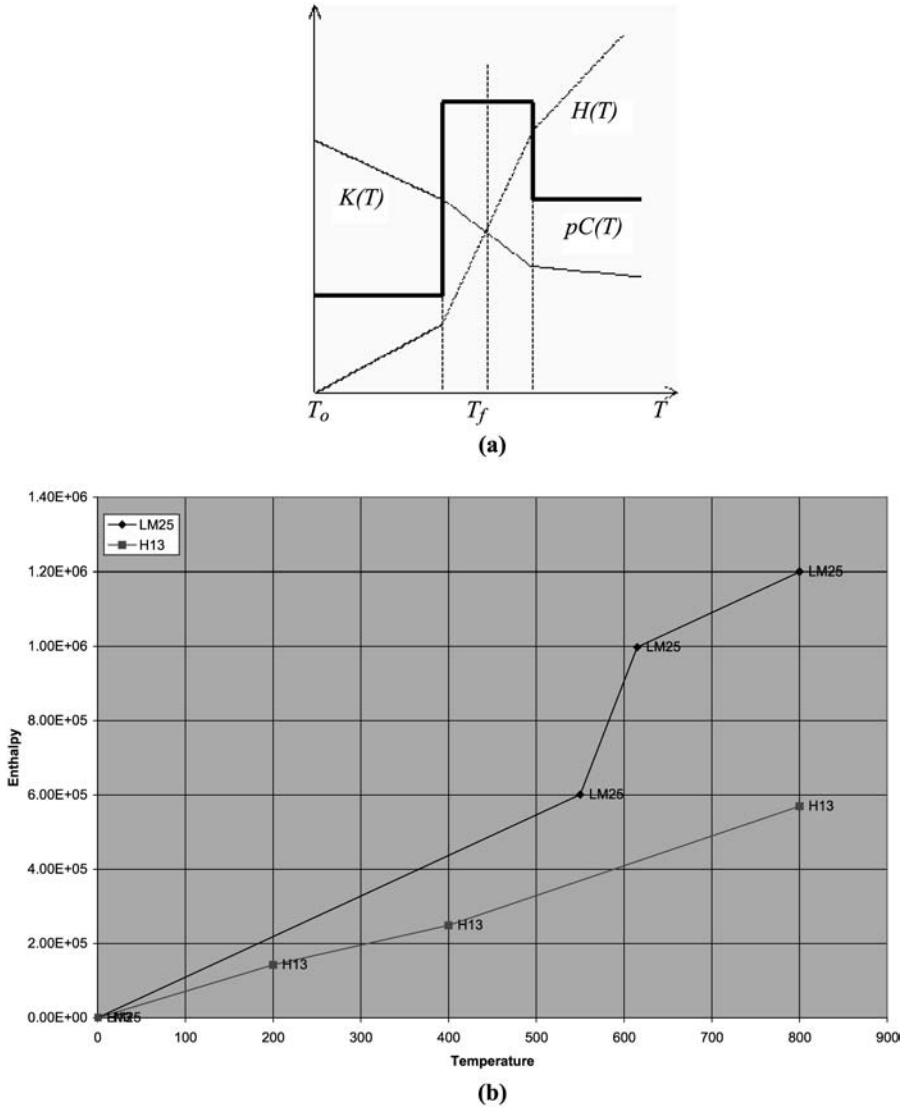

Figure 1.
Illustration of the enthalpy method (a), enthalpy curves used in the examples (b)

transformation and leads to a faster convergence. The enthalpy curves used in the numerical examples are shown in Figure 1(b).

Introducing the new variable H, such that, $\mathrm{d}H/\mathrm{d}T = \rho c_p$ and employing the finite element approximation then equation (9) may be transformed into the following form:

$$\mathbf{K}\mathbf{T}_N + \frac{\mathrm{d}\mathbf{H}}{\mathrm{d}T}\dot{\mathbf{T}}_N = \mathbf{F} \tag{10}$$

The definitions of the enthalpy variable for pure metals and alloys are given by equation (11) as follows:

$$H = \begin{cases} \int c\mathrm{d}T, & T \le T_m \\ \int c\mathrm{d}T + (1 - f_s)\Delta h_f, & T = T_m \\ \int c\mathrm{d}T + \Delta h_f, & T > T_m \end{cases}$$

$$H = \begin{cases} \int c\mathrm{d}T, & T \le T_{\mathrm{sol}} \\ \int c\mathrm{d}T + (1 - f_s)\Delta h_f, & T_{\mathrm{sol}} \le T \le T_{\mathrm{liq}} \\ \int c\mathrm{d}T + \Delta h_f, & T > T_{\mathrm{liq}} \end{cases} \tag{11}$$

The following averaging formula (Lewis *et al.*, 1978) was used for the estimation of the enthalpy variable, i.e.

$$(\rho c_p) \cong \left(\frac{\left(\frac{\partial H}{\partial x}\right)^2 + \left(\frac{\partial H}{\partial y}\right)^2 + \left(\frac{\partial H}{\partial z}\right)^2}{\left(\frac{\partial T}{\partial x}\right)^2 + \left(\frac{\partial T}{\partial y}\right)^2 + \left(\frac{\partial T}{\partial z}\right)^2} \right)^{1/2} \tag{12}$$

The averaging scheme is valid for both mould filling and thermal stress analyses.

3. Mould filling

The metal displacement during the die closure process in squeeze casting is an important process because many defects, such as air entrapment, slag inclusion, cold shuts and cold laps may arise during this process. Modelling the metal displacement requires an efficient approach in order to optimise an existent process or modify a new design. The finite element method has been used successfully in modelling the mould filling process of conventional castings (Usmani *et al.*, 1992, 1993; Lewis *et al.*, 1995, 1997). However, little work has been done on modelling the metal displacement in the squeeze casting process except for the early work by Gethin *et al.* (1992), in which an approximate method was employed to incorporate the effect of the metal displacement in the solidification simulation for squeeze casting processes.

Free surface flow, in a continuously varying die cavity, results from the downward punch movement which is a main feature of the squeeze casting die filling process. The volume of fluid method and its variants are commonly used for the analysis of such free surface problems (Hirt and Nichols, 1981). A scalar function, known as a "pseudo-concentration" function, has been employed for locating the front on a fixed mesh (Usmani *et al.*, 1992, 1993; Lewis *et al.*, 1995; Ravindran and Lewis, 1998). The flow in the entire computational domain can be treated as a single-phase flow with time/space dependent properties, and there is no need to prescribe any boundary condition on the free surface. This fixed mesh approach is known as an Eulerian method. An alternative for dealing with free surface problems is the Lagrangian approach, in which the mesh moves with the fluid (Hirt and Cook, 1970). The Lagrangian method is particularly suited to problems where the mesh does not experience significant distortion, but for most flow problems, the motion of the mesh may lead to unacceptable element entanglement and numerical instability. Hence, the mesh has to be regenerated frequently (Malcevic and Ghattas, 2002). The arbitrary Lagrangian-Eulerian approach, which allows the mesh to move arbitrarily, is a better approach for overcoming excessive mesh distortion (Braess and Wriggers, 2000; Souli and Zolesio, 2001).

In this paper, a quasi-static Eulerian finite element method is presented for modelling the metal displacement in the squeeze casting process. The dynamic metal displacement process is divided into a series of static processes, called subcycles, in each of which the dieset configuration is considered as being in a static state, thus the metal displacement is modelled by solving the Navier-Stokes equation on a fixed mesh. For each subcycle, an individual mesh is created to accommodate the changed dieset configuration due to the motion of the punch. Mesh-to-mesh data mapping is carried out regularly between two adjacent subcycles. The metal front is tracked with the pseudo-concentration method where a first order pure convection equation is solved by using the Taylor-Galerkin method. An aluminium alloy casting was simulated and the numerical results are discussed to assess the effectiveness of the numerical approach.

3.1 Fluid flow and free surface tracking

The flow of liquid metal may be assumed to be Newtonian and incompressible. The governing Navier-Stokes equations, which represent the conservation of mass and momentum, are given below in terms of the primitive flow variables, i.e. the velocity vector $\mathbf{u}$ and pressure p:

$$\nabla \cdot \mathbf{u} = 0 \tag{13}$$

$$\rho\left(\frac{\partial \mathbf{u}}{\partial t} + (\mathbf{u}\cdot\nabla)\mathbf{u}\right) = \nabla \cdot \mu[\nabla\mathbf{u} + (\nabla\mathbf{u})^{\mathrm{T}}] - \nabla p + \rho\mathbf{g} \tag{14}$$

where ρ is the density, p is the pressure, μ is the dynamic viscosity and $\mathbf{g}$ is the gravitational acceleration vector. The free surface movement is governed by the following first order pure advection equation:

$$\frac{\partial F}{\partial t} + (\mathbf{u}\cdot\nabla)F = 0 \tag{15}$$

where F is the pseudo-concentration function, which is defined as a continuous function varying between -1 and 1 across the element lying on the free surface.

Equations (13) and (14) are discretized in space by the conventional Galerkin finite element method. A "mixed" or "integrated" solution approach is adopted, in which the velocity and pressure are computed simultaneously during each iteration. Six-node triangular elements are used with velocity values assigned to all the six nodes, and pressure unknowns considered only for the corner nodes. Equation (15) is discretized by using the Taylor-Galerkin scheme to avoid oscillations which occur when a conventional Galerkin finite element method is adopted. The pseudo-concentration function is approximated by linear shape functions using three-node triangular elements. For this purpose each of the six-node triangular elements used in the flow computation are divided into four three-node sub-elements. An implicit-explicit coupling approach was employed to model the metal flow and free surface evolution. The fluid flow is computed by a fully implicit scheme with a larger time step (Δt). The metal front is tracked by an iterative explicit scheme with a smaller time step (Δt_{exp}) so that the front does not "jump" more than one cell within any time step. Details of the finite element formulation and numerical algorithm can be found in Ravindran and Lewis (1998) and Lewis and Ravindran (2000).

3.2 Modelling of metal displacement

The metal displacement in the die closure process of squeeze casting is a dynamic process where the liquid metal is driven to flow by the continuously downward punch movement.

As a result of the fluid flow, the metal front moves upward in the die cavity and in some cases, where the die has secondary cavities, overspill may also take place. During the process the whole die cavity, including filled and unfilled regions, becomes progressively smaller as the molten metal is forced to frequently relocate in the varying die cavity until the process is finished. Obviously, the metal displacement in the squeeze casting process is very different from the mould filling of conventional casting processes.

As mentioned earlier, an Eulerian type approach has been employed in the present study, which implies that the fluid flow and free surface are computed on a fixed finite element mesh that is placed over the entire domain of the filled and unfilled regions. In order to accommodate the variation of the die cavity, more than one mesh, generally a set of meshes corresponding to different punch positions have to be generated to cover the whole process of the die closure.

Accordingly, the dynamic process of metal displacement is divided into a series of static processes, in each of which a fixed dieset configuration and its corresponding finite element mesh are employed to model the fluid flow and free surface movement. The combination of all the static processes is used to approximately represent the dynamic process. This is the reason why the present method is termed a "quasi-static" approach. Here, each of the static processes is referred to as a "subcycle" and any two adjacent subcycles are linked by appropriate interpolation for velocity, pressure, and the pseudo-concentration function from a previous mesh to subsequent meshes. This procedure is referred to as data mapping in this paper. In addition, it is ensured that the total volume of the molten metal is conserved providing that any volume change caused by cooling and solidification, is negligible. Therefore, a global volume, or mass conservation, must be ensured during the simulation.

3.3 Punch movement simulation

The downward punch movement has two direct consequences. One of them is to change the shape and size of the whole die cavity which can be accommodated by generating a series of finite element meshes as mentioned earlier. The other is to force the molten metal to flow into the die cavity. In the present work, a velocity boundary condition is imposed at the interface between the punch and the liquid metal in order to simulate the effect of the punch action, as shown in Figure 2. This is effectively the prescription of an inlet velocity boundary condition in conventional mould filling simulations. However, this boundary condition is different in respect of the "inlet". In a conventional mould filling process, the position and size of the inlet do not change at all. In contrast, in the squeeze casting process

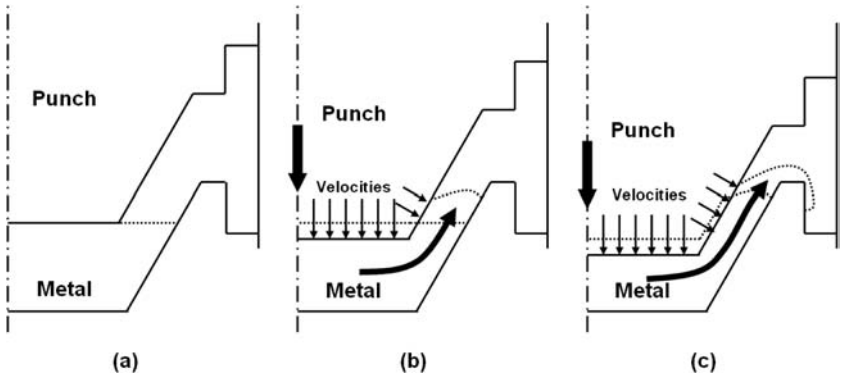

Figure 2.
Schematic illustration of modelling the metal flow in squeeze casting process

the punch/metal interface may vary with the movement of the metal front. This implies that the punch/metal interface, where the velocity boundary condition needs to be prescribed, depends upon the profile of the metal front, which is itself an unknown. Therefore, an iterative solution procedure is employed, in which the status of each node on the punch/metal boundaries is switched "on" or "off" dynamically by referring to its pseudo-concentration function value. Whether the boundary velocity is prescribed depends on the transient status of the nodes.

In practical squeeze casting processes, the punch may be designed to have an arbitrary and generally irregular contour for producing castings, thus satisfying any particular engineering requirements. Consequently, although the punch is actuated to move, in most cases only in the vertical direction and normally with a constant speed, the local impact of the punch on the liquid metal may vary along the contact interfaces. Therefore, the particular direction of the boundary segments must be taken into account in the prescription of the velocity boundary conditions.

3.4 Mesh to mesh data mapping

The mesh-to-mesh data mapping from a previous subcycle to the following one is implemented based on three-noded triangular elements which are generated by sub-dividing six-noded flow elements. As mentioned earlier, the values of velocity and the pseudo-concentration function are assigned to all of the nodes, but the values of pressure are solved only for the corner nodes of the six-node triangular elements. To enable the three-node elements to be used for the data mapping, the pressure values for the mid-side nodes of the flow element are calculated by using a linear interpolation. In the data mapping process, a node-locating procedure, in which all of the new-mesh nodes are located in the old mesh, is followed by a simple linear interpolation based on three-node triangular elements.

3.5 Global mass conservation

The global mass conservation for the molten metal must be guaranteed in the modelling. Based on the above description, the metal mass in the die cavity after the data mapping is less than that at the initial moment. The initial metal mass can be used as a criterion to judge whether it is appropriate to complete an ongoing subcycle and commence a new subcycle. Initially, the total mass of the metal at the onset of the process is calculated and is denoted by M_0. In the computation for each subcycle, the metal mass in the die cavity is monitored after each iterative loop. Once the correct value of M_0 has been attained, the ongoing subcycle is immediately ended and a new subcycle commences.

3.6 Numerical simulation and results

A numerical simulation has been carried out for an aluminum alloy casting. The computer code employed in the simulation is developed based on the mould filling part of the integrated finite element package, MERLIN (Lewis, 1996), which has been tested with benchmark problems for fluid flow (Lewis and Ravindran, 2000).

The initial and final dieset configurations for the casting are shown in Figure 3. As the casting has an axisymmetric geometry, only half of the vertical section of the casting and dieset configuration was considered in the numerical simulation. The outer diameter of the casting is 620 mm, the height 155 mm, and the wall thickness 15-18 mm. The total

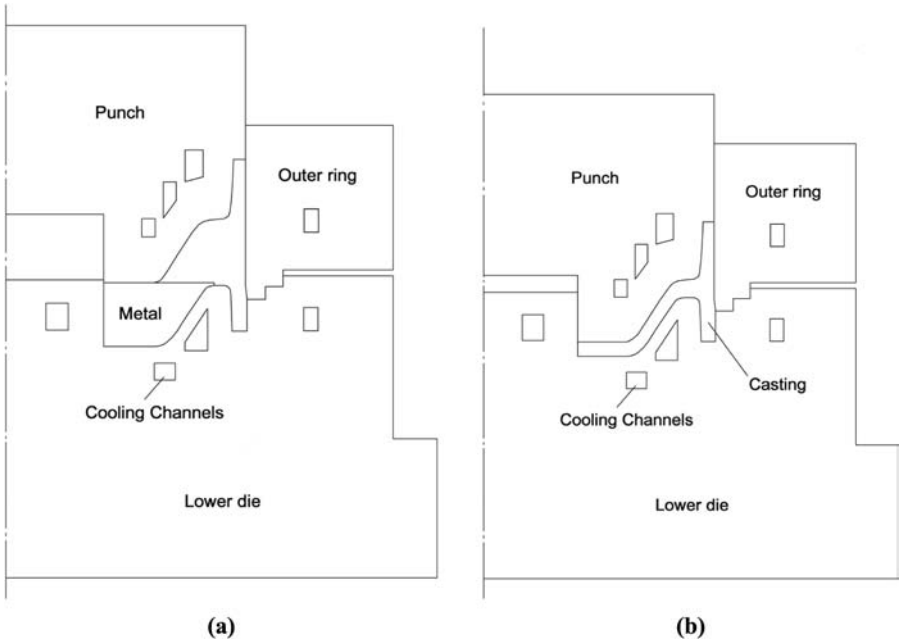

Figure 3.
The initial (a) and final (b) dieset configurations for the casting

displacement of the punch, from its immediate contact on the metal surface to the end of the die closure process, is 58 mm which was divided into thirteen 4 mm displacement increments and two final increments of 3 mm during the simulation. The moving speed of the punch is 10 mm/s and the whole metal displacement process lasts 5.8 s. Some typical meshes of the die cavity for different punch positions are shown in Figure 4.

Figure 5 shows the evolution of the metal profile in the die cavity. The numerical results clearly simulate the process where the liquid metal is displaced in the continuously changing die cavity as a result of the punch action. Figure 6 shows some typical velocity distributions during the die filling process. It is shown that the metal overspill into a secondary cavity can be depicted by the proposed numerical approach. In addition, it can also be seen that, as the process continues, the velocity of the metal flow increases significantly due to the fact that the die cavity space is reduced continuously while the punch keeps on moving at a constant pace. Therefore, optimisation of the punch speed could be an effective approach in improving the flow pattern.

A quasi-static Eulerian finite element method has been presented for modelling the metal displacement in the squeeze casting process. An aluminum alloy casting was modelled and the evolution of the metal profile in the die cavity, as well as the velocity distribution within the melt, are revealed. The numerical approach adopted in this paper has proved to be effective in modelling the squeeze casting process.

4. Mechanical problem

4.1 Equation of equilibrium

The mechanical model is treated as an elasto-viscoplastic system with the assumption of large displacements (Owen and Hinton, 1980; Bathe, 1996).

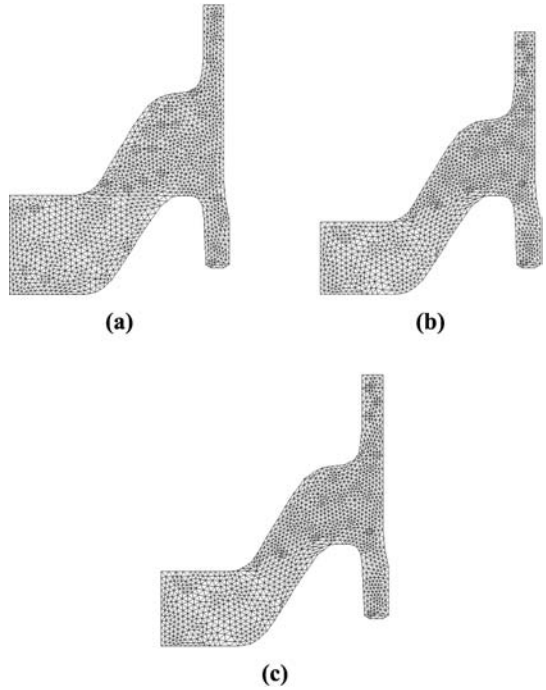

Figure 4.
The mesh of the die cavity for different punch positions: 0 mm (a), 20 mm (b), 40 mm (c)

The influence of initial stresses is enhanced by incorporating a geometrical stiffness matrix.

The total potential energy of the system is of the form:

$$\Pi = \int_{\Omega^o} \frac{1}{2} {}^{t+\Delta t}_{o}\mathbf{S} \cdot {}^{t+\Delta t}_{o}\mathbf{E}\, \mathrm{d}\Omega^o - \int_{\Omega^o} \mathbf{f}^{t+\Delta t}\mathbf{u}\, \mathrm{d}\Omega^o - \int_{\partial\Omega^t_\sigma}^{t+\Delta t} \mathbf{t}^{t+\Delta t}\mathbf{u}\, \mathrm{d}\left(\partial\Omega^t_\sigma\right) \tag{16}$$

where $\mathbf{S}$ and $\mathbf{E}$ are the II Piola-Kirchhof stress tensor and Green Lagrange strains, respectively, $\mathbf{f}$, $\mathbf{t}$ and $\mathbf{u} = \{u, v, w\}$ are body forces, boundary tractions and displacements. All the quantities are determined at time $t + \Delta t$ in the initial configuration (o). Taking the variation of equation (16) we obtain the virtual work equation as follows:

$$\delta\Pi = \int_{\Omega^o} {}^{t+\Delta t}_{o}\mathbf{S} \cdot \delta\, {}^{t+\Delta t}_{o}\mathbf{E}\, \mathrm{d}\Omega^o - \int_{\Omega^o} \mathbf{f}\delta^{t+\Delta t}\mathbf{u}\, \mathrm{d}\Omega^o - \int_{\partial\Omega^o_\sigma}^{t+\Delta t} \mathbf{t}\delta^{t+\Delta t}\mathbf{u}\, \mathrm{d}\left(\partial\Omega^o_\sigma\right) \tag{17}$$

Exploiting the following relations (Malvern, 1969; Crisfield, 1991):

$${}^{t+\Delta t}_{o}\mathbf{S} = \frac{\rho}{\rho_o} {}^{t+\Delta t}_{t}\mathbf{S}, \quad {}^{t+\Delta t}_{o}\mathbf{E} = \frac{\rho}{\rho_o} {}^{t+\Delta t}_{t}\mathbf{E}, \quad \rho\, \mathrm{d}\Omega^t = \rho_o\, \mathrm{d}\Omega^o \tag{18}$$

we transform the above virtual work equation, equation (17), to the configuration at time t (in the spirit of the updated Lagrangian approach). The equation reads:

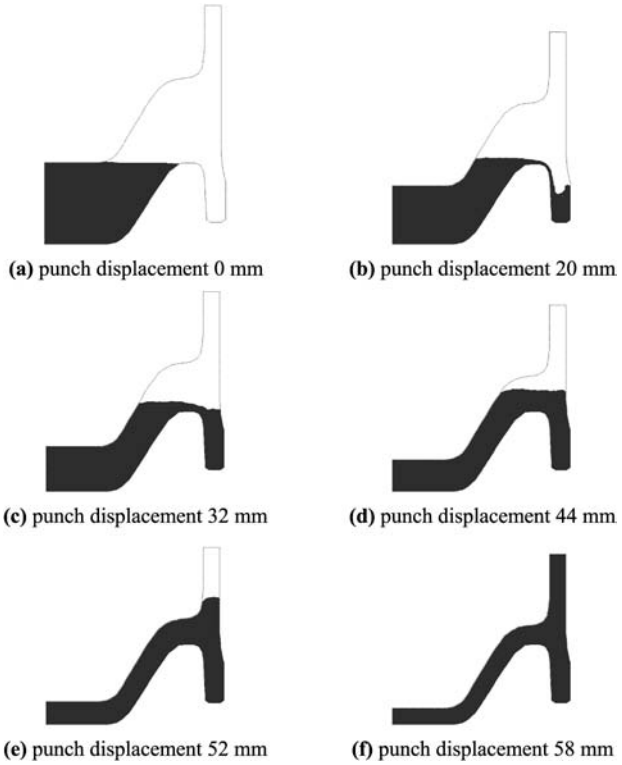

Figure 5.
The evolution of the metal profile in the die cavity

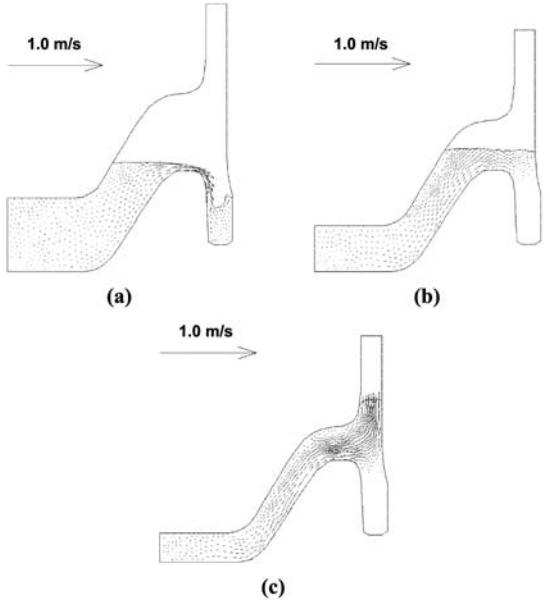

Figure 6.
Typical velocity distribution during the die closure process: 20 mm (a), 40 mm (b), 52 mm (c)

$$\int_{\Omega^t} {}^{t+\Delta t}_{t}\mathbf{S}\cdot\delta\,{}^{t+\Delta t}_{t}\mathbf{E}\,\mathrm{d}\Omega^t = \int_{\Omega^t}{}^{t+\Delta t}\mathbf{t}\delta^{t+\Delta t}\mathbf{u}\,\mathrm{d}\Omega^t + \int_{\partial\Omega^t_\sigma}{}^{t+\Delta t}\mathbf{t}\delta^{t+\Delta t}\mathbf{u}\,\mathrm{d}\left(\partial\Omega^t_\sigma\right) \tag{19}$$

Now, the goal becomes one of obtaining the final form of the virtual work equation before discretization takes place. To achieve this the following incremental decomposition is employed:

$$\begin{gathered}{}^{t+\Delta t}_{t}\mathbf{E} = {}^{t}_{t}\mathbf{E} + \Delta\mathbf{E},\quad {}^{t+\Delta t}_{t}\mathbf{S} = {}^{t}_{t}\mathbf{S} + \Delta\mathbf{S},\quad {}^{t+\Delta t}\mathbf{u} = {}^{t}\mathbf{u} + \Delta\mathbf{u},\quad {}^{t+\Delta t}\mathbf{f} = {}^{t}\mathbf{f} + \Delta\mathbf{S},\\ {}^{t+\Delta t}\mathbf{t} = {}^{t}\mathbf{t} + \Delta\mathbf{t}\end{gathered} \tag{20}$$

along with the following relations for stress increments (${}^{t}_{t}\boldsymbol{\tau}$ is the Cauchy stress tensor) and the strain increment decomposition into its linear and nonlinear parts, i.e.

$${}^{t}_{t}\mathbf{S} = {}^{t}_{t}\boldsymbol{\tau},\quad {}^{t+\Delta t}_{t}\mathbf{S} = {}^{t}_{t}\boldsymbol{\tau} + \Delta\mathbf{S},\quad \Delta\mathbf{E} = \Delta\mathbf{e} + \Delta\boldsymbol{\eta},\quad \Delta\mathbf{e} = \overline{\mathbf{A}}\Delta\mathbf{u},\quad \Delta\boldsymbol{\eta} = \frac{1}{2}\bar{\bar{\mathbf{A}}}(\Delta\mathbf{u}')\Delta\mathbf{u}' \tag{21}$$

where $\Delta\mathbf{u}'$ is the vector of the displacement increment derivatives w.r.t. Cartesian coordinates and $(\bar{\mathbf{A}}, \bar{\bar{\mathbf{A}}})$ are the linear and nonlinear operators as follows:

$$\bar{\mathbf{A}} = \begin{bmatrix} \frac{\partial}{\partial x} & 0 & 0\\ 0 & \frac{\partial}{\partial y} & 0\\ 0 & 0 & \frac{\partial}{\partial z}\\ \frac{\partial}{\partial y} & \frac{\partial}{\partial x} & 0\\ \frac{\partial}{\partial z} & 0 & \frac{\partial}{\partial x}\\ 0 & \frac{\partial}{\partial z} & \frac{\partial}{\partial y} \end{bmatrix}$$

$$\bar{\bar{\mathbf{A}}} = \begin{bmatrix} \Delta u'_x & 0 & 0 & \Delta v'_x & 0 & 0 & \Delta w'_x & 0 & 0\\ 0 & \Delta u'_y & 0 & 0 & \Delta v'_y & 0 & 0 & \Delta w'_y & 0\\ 0 & 0 & \Delta u'_z & 0 & 0 & \Delta v'_z & 0 & 0 & \Delta w'_z\\ \Delta u'_y & \Delta u'_x & 0 & \Delta v'_y & \Delta v'_x & 0 & \Delta w'_y & \Delta w'_x & 0\\ 0 & \Delta u'_z & \Delta u'_y & 0 & \Delta v'_z & \Delta v'_y & 0 & \Delta w'_z & \Delta w'_y\\ \Delta u'_z & 0 & \Delta u'_x & \Delta v'_z & 0 & \Delta v'_x & \Delta w'_z & 0 & \Delta w'_x \end{bmatrix} \tag{22}$$

Substituting equations (18), (20), (21) into the virtual work equation, equation (19) we arrive at:

$$\int_{\Omega^t} \left({}_t^t\boldsymbol{\tau}\cdot\delta\boldsymbol{\eta} + \Delta\mathbf{S}\cdot\delta\Delta\mathbf{e}\right)\mathrm{d}\Omega^t = \int_{\Omega^t}^{t+\Delta t} \mathbf{f}\delta^{t+\Delta t}\mathbf{u}\,\mathrm{d}\Omega^t + \int_{\partial\Omega_\sigma^t}^{t+\Delta t} \mathbf{t}\delta^{t+\Delta t}\mathbf{u}\,\mathrm{d}\left(\partial\Omega_\sigma^t\right) - \int_{\Omega^t} {}_t^t\boldsymbol{\tau}\cdot\delta\Delta\mathbf{e}\,\mathrm{d}\Omega^t \tag{23}$$

Equation (23) is solved iteratively, however, for brevity we assume that the equation is fulfilled precisely at time t and as a result we obtain the following incremental form of the virtual work equation:

$$\int_{\Omega^t} \left({}_t^t\boldsymbol{\tau}\cdot\delta\boldsymbol{\eta} + \Delta\mathbf{S}\cdot\delta\Delta\mathbf{e}\right)\mathrm{d}\Omega^t = \int_{\Omega^t} \Delta\mathbf{f}\delta\Delta\mathbf{u}\,\mathrm{d}\Omega^t + \int_{\partial\Omega_\sigma^t} \Delta\mathbf{t}\delta\Delta\mathbf{u}\,\mathrm{d}\left(\partial\Omega_\sigma^t\right) \tag{24}$$

Employing the finite element approximation:

$$\Delta\mathbf{u} = \mathbf{N}\Delta\mathbf{q}, \quad \Delta\mathbf{u}' = \mathbf{B}'_L\Delta\mathbf{q} \tag{25}$$

where $\mathbf{N}$ is the set of shape functions, $\Delta\mathbf{q}$ is the increment of nodal displacements and considering the following set of equalities, i.e.

$${}_t^t\boldsymbol{\tau}^{\mathrm{T}}\delta\boldsymbol{\eta} = {}_t^t\tau\delta\left(\bar{\bar{\mathbf{A}}}\right)\Delta\mathbf{u}' = \delta(\Delta\mathbf{u}')^{\mathrm{T}}\,{}_t^t\bar{\tau}\Delta u' = \delta(\Delta\mathbf{q})^{\mathrm{T}}\,{}_t^t\bar{\boldsymbol{\tau}}\mathbf{B}'_L \tag{26}$$

where ${}_t^t\bar{\boldsymbol{\tau}}$ is the Cauchy stress matrix:

$${}_t^t\bar{\boldsymbol{\tau}} = \begin{bmatrix} {}_t^t\underline{\boldsymbol{\tau}} & & \\ & {}_t^t\underline{\boldsymbol{\tau}} & \\ & & {}_t^t\underline{\boldsymbol{\tau}} \end{bmatrix} \quad {}_t^t\underline{\boldsymbol{\tau}} = \begin{bmatrix} {}_t^t\sigma_{xx} & {}_t^t\boldsymbol{\tau}_{xy} & {}_t^t\boldsymbol{\tau}_{xz} \\ & {}_t^t\sigma_{yy} & \boldsymbol{\tau}_{yz} \\ & & {}_t^t\sigma_{zz} \end{bmatrix} \tag{27}$$

we obtain the following discretized form of the virtual work equation:

$$\left(\int_{\Omega^t} \mathbf{B}'^{\mathrm{T}}_L\,{}_t^t\bar{\boldsymbol{\tau}}\mathbf{B}'_L\,\mathrm{d}\Omega^t\right)\Delta\mathbf{q} + \int_{\Omega^t} \mathbf{B}_L^T\Delta\mathbf{S}\,\mathrm{d}\Omega^t = \int_{\Omega^t} \mathbf{N}^{\mathrm{T}}\Delta\mathbf{f}\,\mathrm{d}\Omega^t + \int_{\partial\Omega_\sigma^t} \mathbf{N}^{\mathrm{T}}\Delta\mathbf{t}\,\mathrm{d}\left(\partial\Omega_\sigma^t\right) \tag{28}$$

Now, we will deal with the constitutive model and employ the linearized constitutive equation of the form:

$$\Delta\mathbf{S} = \mathbf{D}(\Delta\varepsilon - \Delta\varepsilon^{vp} - \Delta\varepsilon^{\mathrm{T}}) \tag{29}$$

The viscoplastic strain increment (Perzyna, 1971), starting from the viscoplastic strain rate evaluation, is calculated as follows:

$$\varepsilon^{vp} = \gamma < \varphi(F) > \frac{\partial Q}{\partial S}, \quad \langle\varphi(F)\rangle = \begin{cases} 0 & F \le 0 \\ \varphi(F) & F > 0 \end{cases} \tag{30}$$

where F and Q are the yield and plastic potential functions, γ is the fluidity parameter and φ is a function defined in the McAuley brackets. When $F = Q$ the plasticity model becomes associative which is the form assumed here. Taking into account a generalized trapezoidal integration rule over time we obtain:

$$\Delta\boldsymbol{\varepsilon}^{vp} = \Delta t[(1-\theta)\dot{\boldsymbol{\varepsilon}}^{vp,n} + \theta\dot{\boldsymbol{\varepsilon}}^{vp,n+1}] \tag{31}$$

On applying a Taylor series expansion to calculate the viscoplastic strain rate at time $n+1$, we obtain:

$$\dot{\boldsymbol{\varepsilon}}^{vp,n+1} = \dot{\boldsymbol{\varepsilon}}^{vp,n} + \left(\frac{\partial\dot{\boldsymbol{\varepsilon}}^{vp}}{\partial\mathbf{S}}\right)^{n}\Delta\mathbf{S}^{n} \tag{32}$$

Stepping further, the viscoplastic strain increment takes the form:

$$\Delta\boldsymbol{\varepsilon}^{vp} = \dot{\boldsymbol{\varepsilon}}^{vp,n}\Delta t + \mathbf{C}^{n}\Delta\mathbf{S}^{n}, \quad \mathbf{C}^{n} = \theta\Delta t\left(\frac{\partial\dot{\boldsymbol{\varepsilon}}^{vp}}{\partial\mathbf{S}}\right)^{n} \tag{33}$$

on employing the finite element discretization to the strain increment, such that $\Delta\boldsymbol{\varepsilon} = \mathbf{B}_L\Delta\mathbf{q}$ and substituting equation (33) into equation (29), we arrive at:

$$\Delta\mathbf{S} = \check{\mathbf{D}}(\mathbf{B}_L\Delta\mathbf{q} - \dot{\boldsymbol{\varepsilon}}^{vp}\Delta t - \boldsymbol{\alpha}\Delta T) \tag{34}$$

where $\check{\mathbf{D}}$ is the the matrix of the form: $\check{\mathbf{D}} = (\mathbf{I} + \mathbf{DC})^{-1}\mathbf{D}$, $\boldsymbol{\alpha}$ is the vector of thermal expansion coefficients and ΔT is the increment of temperature.

Substituting the constitutive equation into the discretized virtual work equation we obtain:

$$\left(\int_{\Omega^t}\mathbf{B'}_{L_t^t}\bar{\boldsymbol{\tau}}\mathbf{B'}_L\,\mathrm{d}\Omega^t\right)\Delta q + \left(\int_{\Omega}\mathbf{B}_L^T\check{\mathbf{D}}\mathbf{B}\,\mathrm{d}\Omega\right)\Delta\mathbf{q} = \Delta\mathbf{f} + \Delta\mathbf{t} + \int_{\Omega}\mathbf{B}\check{\mathbf{D}}\dot{\boldsymbol{\varepsilon}}^{vp}\Delta\mathbf{t}\,\mathrm{d}\Omega + \int_{\Omega}\check{\mathbf{D}}\boldsymbol{\alpha}\Delta T\,\mathrm{d}\Omega \tag{35}$$

Equation (35) is finally solved using the Newton Raphson method.

4.2 Interfacial heat transfer coefficient

In our case the interfacial heat transfer coefficient is used for establishing the interface thermal properties of the layer between the mould and the casting. The inclusion of this effect is critical in solidification processes because of the pressure and airgap effects.

The interfacial heat transfer coefficient depends on the air conductivity (k_{air}), thermal properties of the interfacing materials and the magnitude of the gap (g). The formula given by Lewis and Ransing (1998, 2000) is adopted: $h = k_{\text{air}}/(g + k_{\text{air}}/h_o)$.

The value of h_o, an initial heat transfer coefficient, should be obtained from experiment and reflects the influence of the type of interface materials where coatings may be applied. Additionally, from a numerical point of view, this allows us to regularize the dependence of the resulting interfacial heat transfer coefficient on the gap magnitude. This dependence is also a source of coupling between the thermal and mechanical equations.

4.3 Contact between casting and mould

The basic assumption is that the whole casting is in perfect contact with the mould at the beginning of the thermal stress analysis. The assumption is justified by the fact that the thermal stress analysis starts after the commencement of solidification. Because of the assumption of small deformations theory we may consider that "node to node" contact occurs. The penalty formulation is used which is briefly described as follows.

Considering the potential energy of an augmented mechanical system where, except for the standard stiffness matrix (linear or nonlinear) $\mathbf{K}$ and forces $\mathbf{F}$, there exists a system of constraints represented by the stiffness $\boldsymbol{\lambda}$. The constraints act between the contacting bodies.

Calculating the potential energy of the system and then minimizing the energy we arrive at an augmented system of equations by taking into account contact interactions, i.e.

$$\Pi = \frac{1}{2}\mathbf{q}^{\mathrm{T}}\mathbf{K}\mathbf{q} - \mathbf{q}^{\mathrm{T}}\mathbf{F} + \frac{1}{2}\mathbf{g}^{\mathrm{T}}\boldsymbol{\lambda}\mathbf{g} \quad \mathbf{K}'q = \mathbf{F}' \tag{36}$$

The term $\mathbf{g}$ is a vector representing the penetration of contacting nodes into the contact surface, $\mathbf{K}'$ and $\mathbf{F}'$ are the augmented stiffness matrix and equivalent force vector, respectively. In the case of non-existence of any contact the distance between the nodes is calculated and in consequence the value is transferred to the thermal module where the interfacial heat transfer coefficient is then calculated.

The penalty number is an input data. In our implementation the possibility of keeping an assumed stiffness is maintained even in the absence of contact between the nodes under consideration. This is due to the fact that for the case of a relatively sudden extensive gap formation some convergence problems may arise and the additional stiffness may accelerate the solution without any significant lost of precision.

4.4 Coupling strategy

A staggered scheme was adopted for the two field problems (thermal and mechanical), as presented by Felippa and Park (1980) and Vaz and Owen (1996). The general scheme for this type of problem is shown in Figure 7. The solution is obtained by sequential execution of two modules (thermal and mechanical).

In the examples analysed, the temperature field is passed to the mechanical module thus affecting the loading, constitutive parameters and the contact conditions. The air-gap, based on the calculated displacement field and actual contact conditions, is transferred from the mechanical to the thermal module.

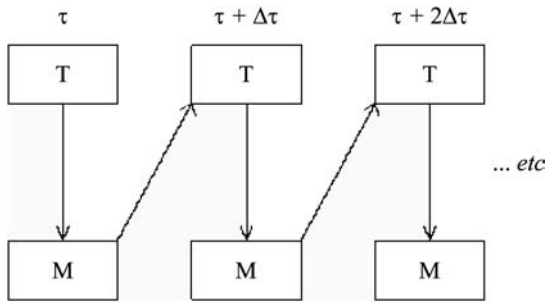

Figure 7.
Coupling strategy

4.5 Cylinder

In order to demonstrate the influence of the applied pressure on the solidification process a cylindrical sample was investigated. The diameter of the mould is 0.084 m, the diameter of the casting is 0.034 m, the height of the casting is 0.075 m and the height of the mould is 0.095 m, respectively.

The sample was discretized with 9,140 isoparametric linear bricks and 10,024 nodes. The finite element mesh for half the cylinder (even though the whole cylinder was analysed) is shown in Figure 8(a). The following thermal boundary and initial conditions were assumed: a constant temperature of 20°C on the outer surface of the

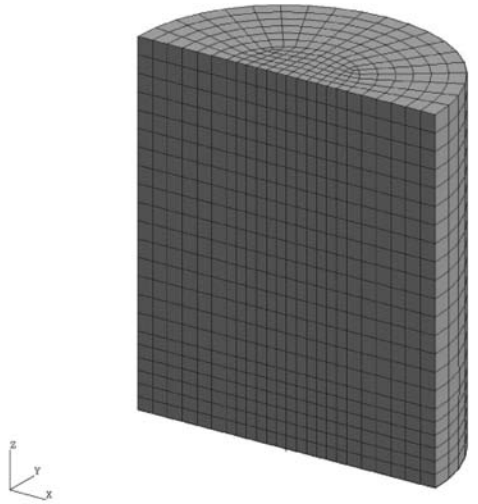

(a)

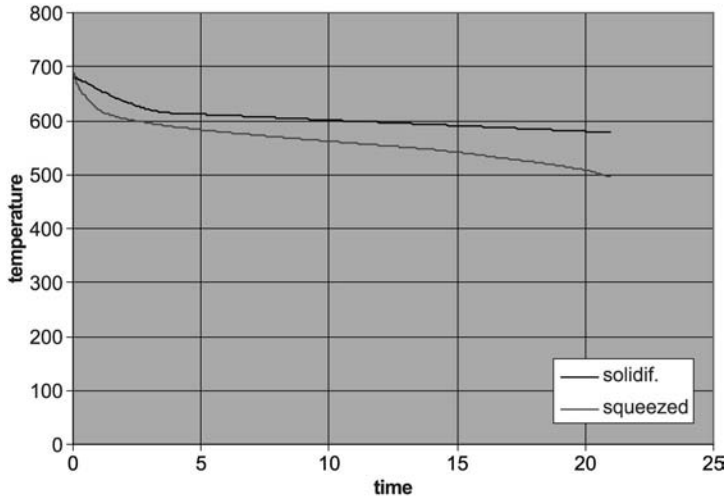

(b)

Figure 8.
Discretized mould and cast (a), temperature variation close to the bottom of the cast; squeezed and free casting (b)

mould, 200°C on the top of the casting, 700°C being the initial temperature of the casting and 200°C the initial temperature of the mould, respectively. The mould is fixed rigidly to the foundation. The die is made of steel H13 with the properties: Young modulus $0.25 \times 10^{12}\,\mathrm{N/m^2}$, Poisson's ratio 0.3, density 7,721 kg/m^3, yield stress $0.55 \times 10^{10}\,\mathrm{N/m^2}$, thermal exp. coeff. 0.12×10^{-5} and the material properties of the casting (aluminium alloy, LM25): Young modulus $0.71 \times 10^{11}\,\mathrm{N/m^2}$, Poisson's ratio 0.3, density 2,520 kg/m^3, yield stress $0.15 \times 10^{9}\,\mathrm{N/m^2}$, fluidity parameter 0.1×10^{-2}, thermal exp. coeff. 0.21×10^{-4}, contraction 0.3×10^{-12}, $T_{\mathrm{liq}} = 612\,\mathrm{C}$, $T_{\mathrm{sol}} = 532\,\mathrm{C}$.

The effect of pressure when applied to the top of the casting is shown in Figure 8(b) and 9. It may be seen that the temperature close to the bottom is lower for the squeezed part than for the casting without external pressure (Figure 8(b)). This is due to the gap closure and subsequent higher interfacial heat transfer coefficient. When comparing the displacement patterns for both cases it is seen that the displacements for the squeezed workpiece are the smallest at the bottom where the gap has closed (Figure 9(c) and (d)). This result implies a higher cooling rate and in consequence faster solidification, the solidified region being larger for the squeezed part (Figure 9(a)) than for the free one (Figure 9(b)).

4.6 Aluminium part – influence of large displacements and initial stresses

An aluminium component was also analysed having overall dimensions of $0.47 \times 0.175 \times 0.11$ m. The component was discretized with 2,520 linear bricks and 3,132 nodes. The thermal boundary and initial conditions were assumed to be the same as for the previous case. The mould is fixed rigidly to the foundation and the pressure is applied to the top of the casting. The material data set is identical to the previously analysed example.

The process is simulated over the first 30 s of the cooling cycle. Results concerning three different cases are shown in Figures 10(a)-(b) and 11. We focus our attention on the solidification patterns. If we assume small displacements it is observed that the effect of pressure is significant, namely, the solidification is much more advanced when applying pressure than for the case of a free casting (Figure 10(a) and (b)). If the influence of nonlinear geometry is included (Figure 11), then the solidification appears to be less advanced than for the case where this effect is ignored (Figure 10(a)). However, the solidification is still more advanced for the case of squeeze forming than for the same component without the influence of an applied external pressure.

4.7 Effect of void

The next example concerns the effect of a void which could appear in a cylindrical casting part. This void could have been created during the mould filling stage. The mould and casting are discretized using 24,072 nodes and 21,232 elements and only a half of the mould is shown in Figure 12.

Two cases are considered, namely, the case of an ideal casting and an imperfect one (with the void). The solidification pattern for the casting with the void at a time 110 s is shown in Figure 12(b), where the void is located in the lower right corner of the casting. The solidification pattern may be seen to be unsymmetric. The solidification pattern for the ideal case is not presented since the casting has already solidified. The Mises stress patterns in the casting and the die are shown in Figures 13 and 14, respectively.

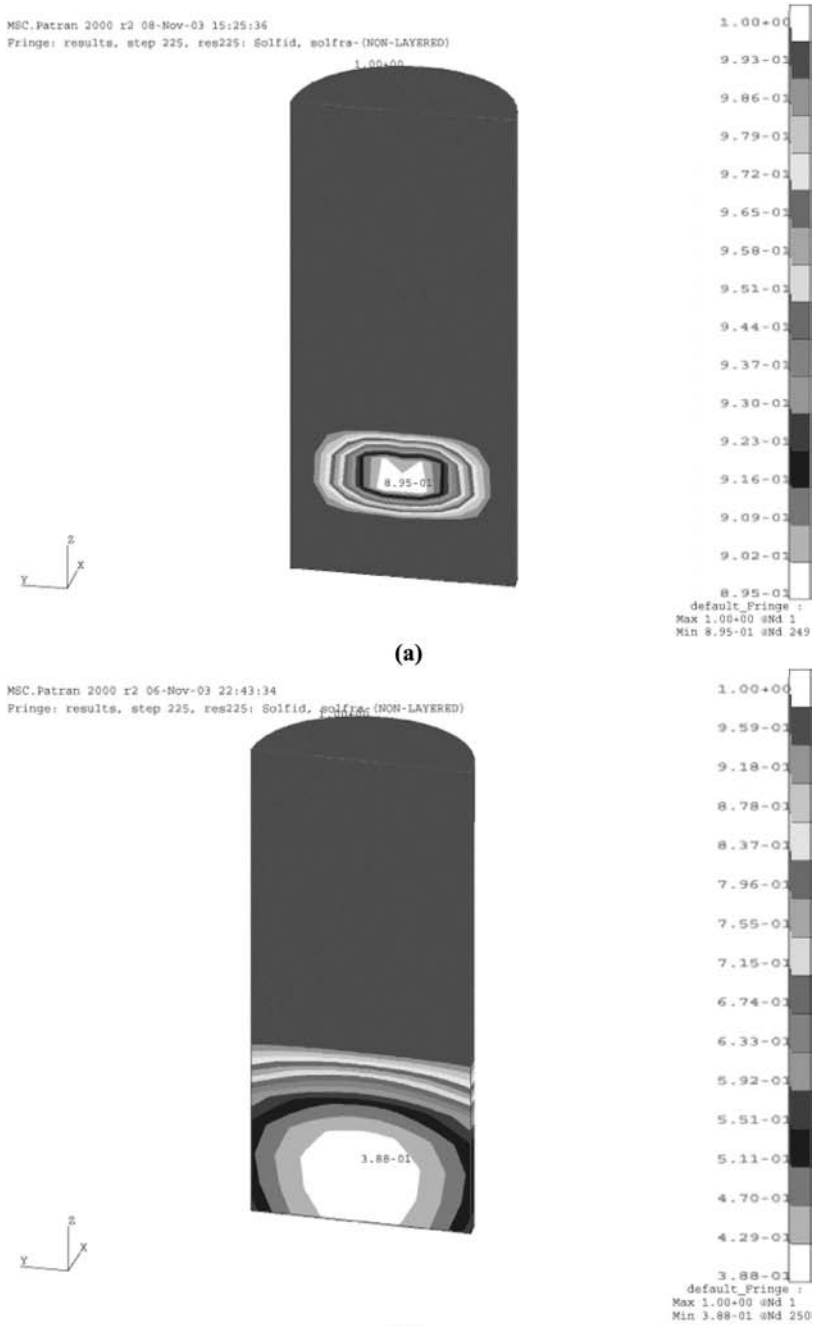

Figure 9.
Solidification (a, b) and displacement (c, d) patterns (squeeze casting – (a, c), no external pressure – (b, d)

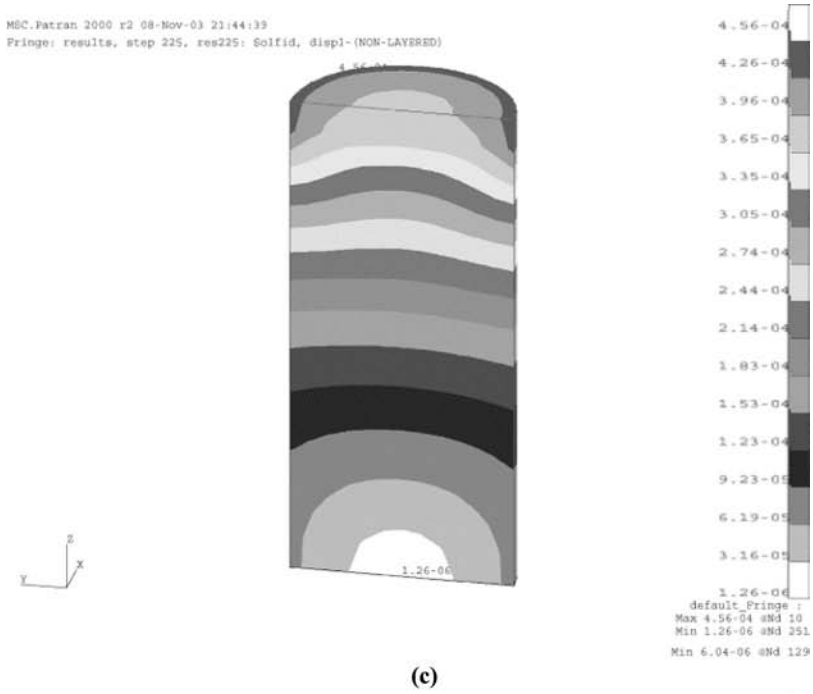
MSC.Patran 2000 r2 08-Nov-03 21:44:39
Fringe: results, step 225, res225: Solfid, displ-(NON-LAYERED)
4.56-04
4.26-04
3.96-04
3.65-04
3.35-04
3.05-04
2.74-04
2.44-04
2.14-04
1.83-04
1.53-04
1.23-04
9.23-05
6.19-05
3.16-05
1.26-06
default_Fringe :
Max 4.56-04 @Nd 10
Min 1.26-06 @Nd 251
Min 6.04-06 @Nd 129
(c)
MSC.Patran 2000 r2 08-Nov-03 21:22:05
Fringe: results, step 225, res225: Solfid, displ-(NON-LAYERED)
2.83-04
2.64-04
2.46-04
2.28-04
2.09-04
1.91-04
1.72-04
1.54-04
1.35-04
1.17-04
9.83-05
7.99-05
6.14-05
4.30-05
2.45-05
6.04-06
default_Fringe :
Max 2.83-04 @Nd 10
Min 6.04-06 @Nd 129
(d)

Figure 9.

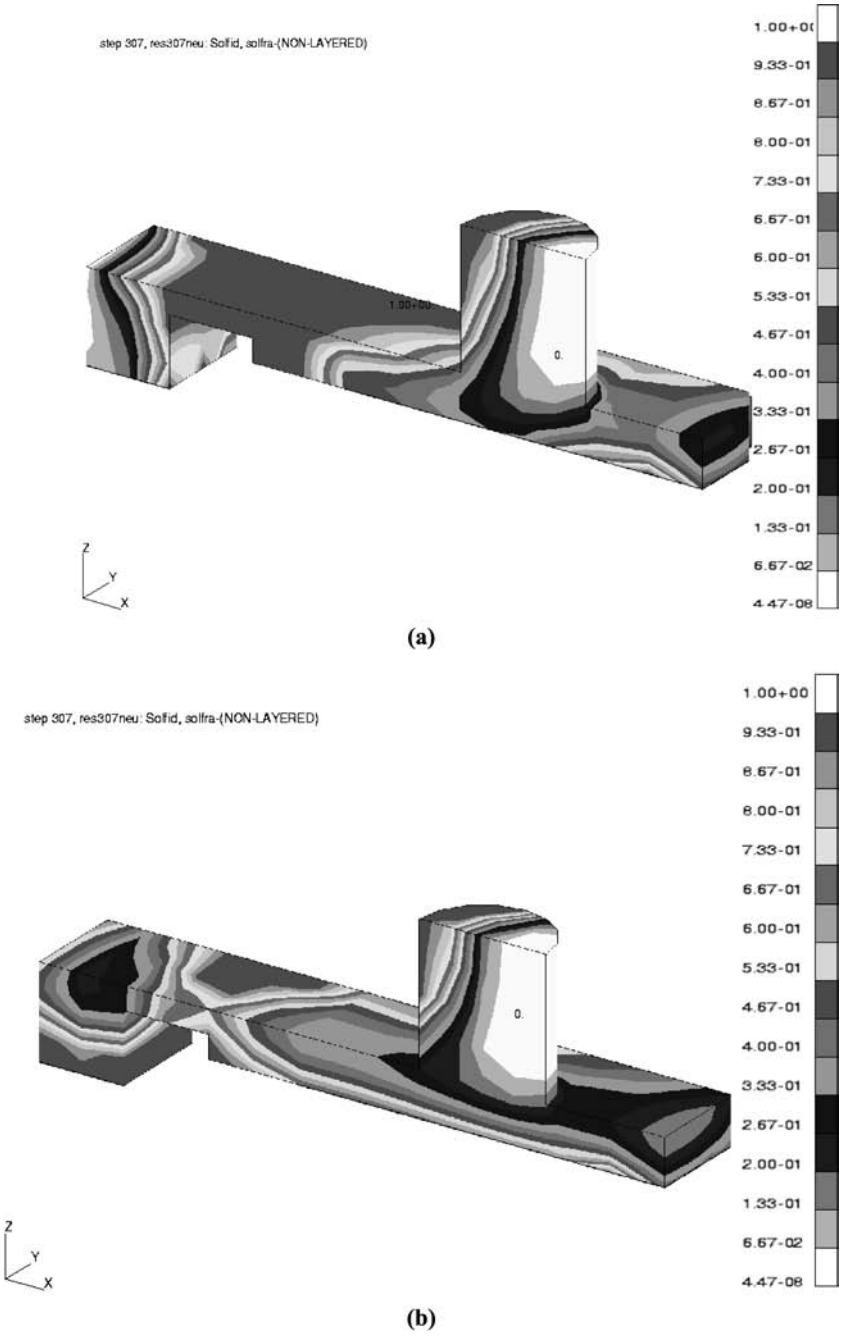

Figure 10.
No external pressure (a), squeeze casting, small displacements (b)

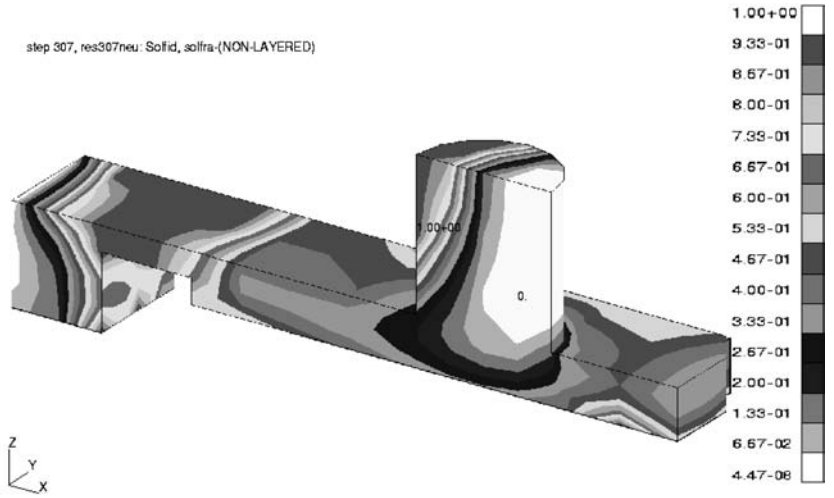

Figure 11.
Squeeze casting (large displacements)

On comparing the ideal and imperfect system it can be seen that the Mises stress patterns are unsymmetric for the imperfect system and also stress concentrations appear in the bottom of the die.

5. Microstructural solidification model

During the entire process of forming a casting component solidification gradually occurs. A microstructure based solidification model has been employed which results in a better understanding of the process. The model stems from the assumptions given by Thevoz *et al.* (1989) and Celentano (2002). The basic assumptions are as follows: the sum of the solid and liquid fractions is equal to one and the solid fraction consists of both dendritic and eutectic fractions, i.e.

$$f_l + f_s = 1, \quad f_s = f_d + f_e \tag{37}$$

Further assumptions are utilised because of the existence of interdendritic and intergranular eutectic fractions. The indices (d, e) denote the dendritic and eutectic fractions. The internal fraction consists of both the dendritic and eutectic portions, i.e.

$$f_s = f_g^d f_i + f_g^e, \quad f_i = f_i^d + f_i^e \tag{38}$$

The last assumptions lead to the final formulae for the dendritic and eutectic fractions (a spherical growth is assumed):

$$f_d = f_g^d f_i^d, \quad f_e = f_g^d f_i^e + f_g^e, \quad f_g^e = \frac{4}{3}\Pi N_d R_d^3, \quad f_i^e = \frac{4}{3}\Pi N_e R_e^3 \tag{39}$$

where N_d, N_e are the grain densities and R_d, R_e are the grain radii. The grain densities and grains sizes are governed by nucleation and growth evolution laws. The rate of growth of the dendritic and eutectic nuclei is given below. This depends on the undercooling $\Delta T_{N(d,e)}$ and a Gaussian distribution $\Delta T_{\sigma(d,e)}$ of the nuclei is assumed.

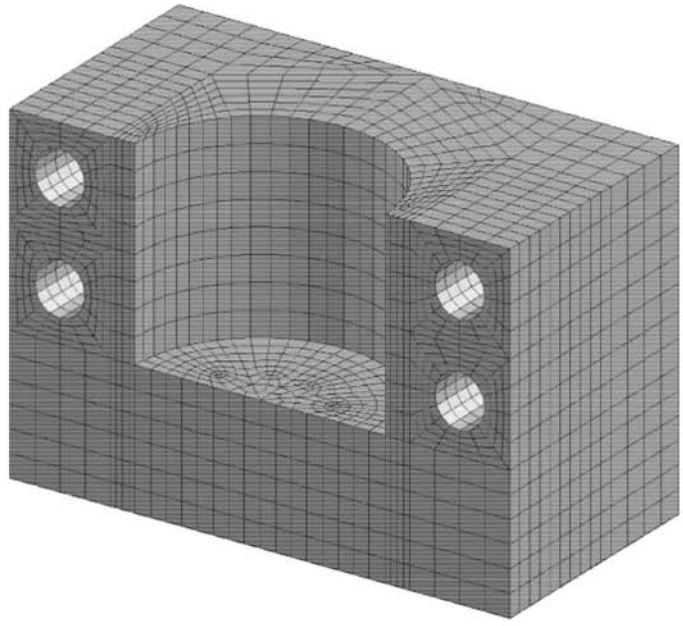

(a)

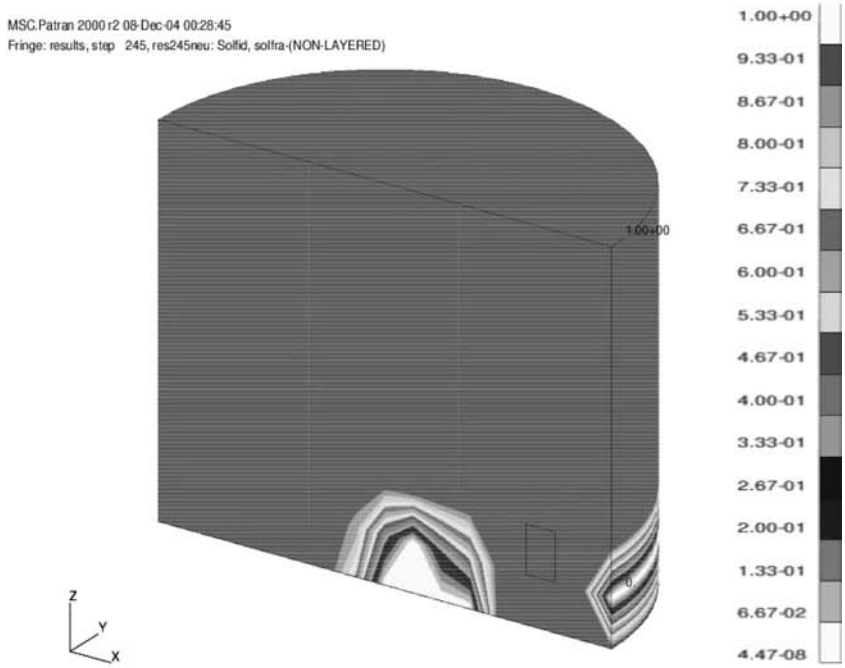

(b)

Figure 12.
Mould (a) and solidification pattern (b), 110 s

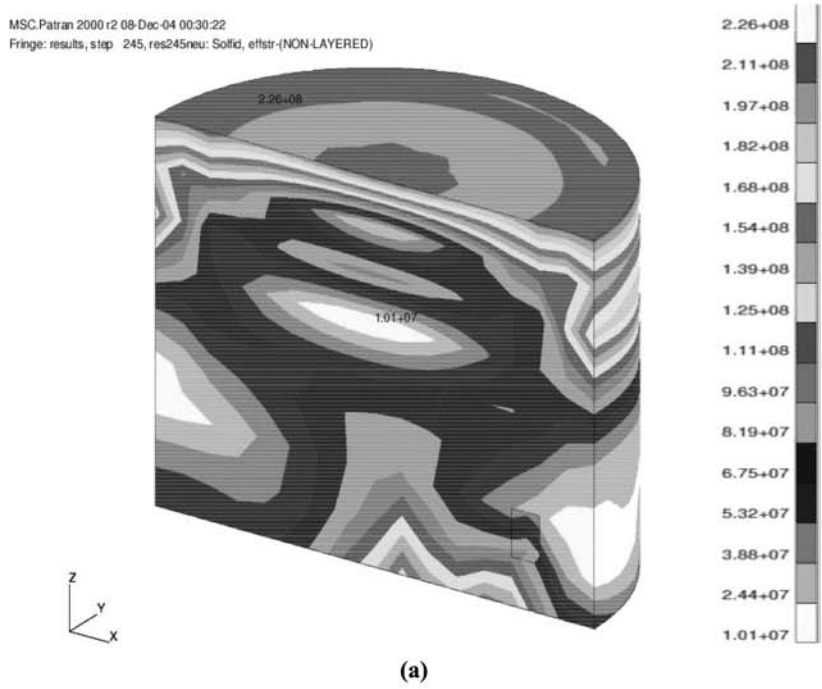

(a)

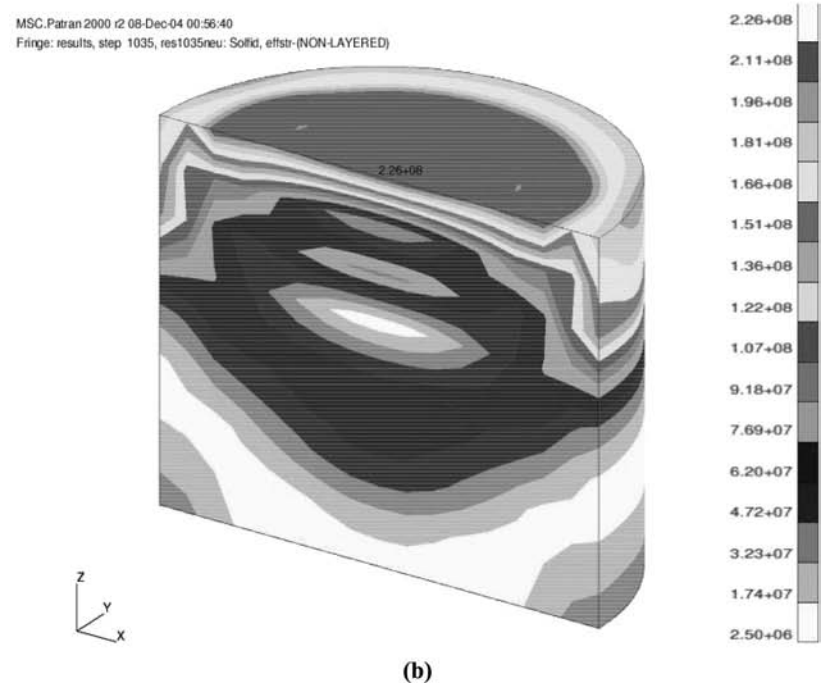

(b)

Figure 13.
Mises stress distribution in the cast: imperfect system (a), ideal (b)

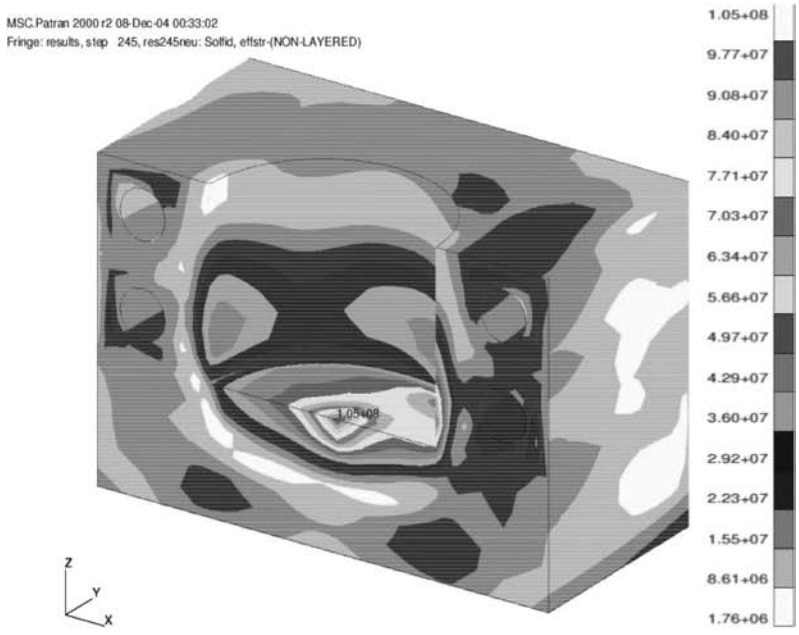

(a)

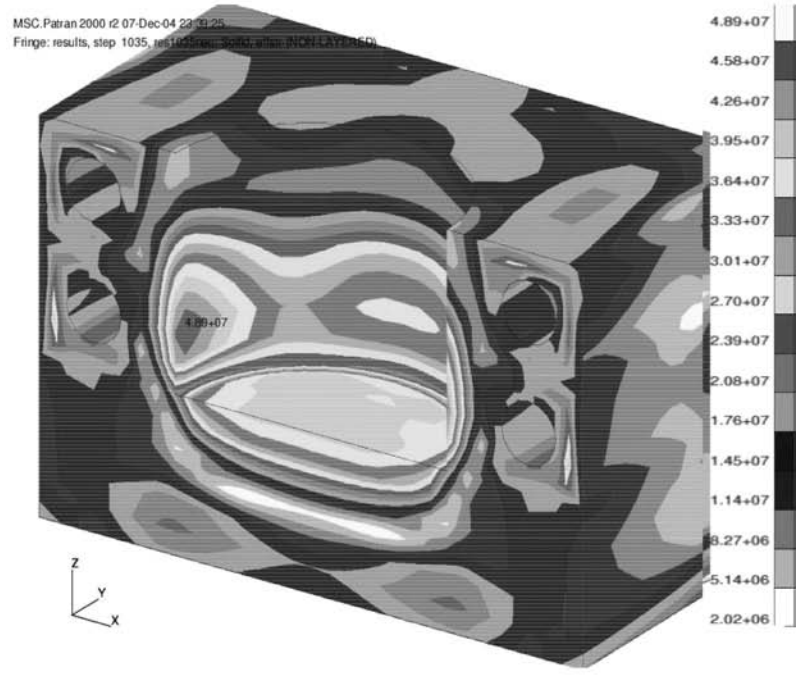

(b)

Figure 14.
Mises stress distribution in the mould: imperfect system (a), ideal (b)

$$\dot{N}_{(d,e)} = N_{\max(d,e)} \frac{1}{2\Pi} \exp\left(-\frac{\Delta T - \Delta T_{N(d,e)}}{2\Delta T_{\sigma(d,e)}}\right) \langle -\dot{T} \rangle, \quad \Delta T_{(d,e)} = T_{(d,e)} - T \tag{40}$$

The McAuley brackets indicate the irreversibility of the process. $N_{\max(d,e)}$ are the grain densities under complete saturation condition.

The rates of the dendritic and eutectic grain radii is established based on experimental dependence. Finally, the internal dendritic fraction depends on the melting temperature and k' is the partition coefficient.

$$\dot{R}_{(d,e)} = f_{R(d,e)}, \quad f_i^d = 1 - \left(\frac{T_m - T}{T_m - T_l}\right)^{\frac{1}{k'-1}} \tag{41}$$

Two numerical examples concerning mould filling and thermal stress analysis are provided.

5.1 Mould filling (microstructural solidification)

A simulation was carried out of the mould filling of an aluminium part (valve), employing the above solidification model. The material of the mould is steel H13 and the casting is aluminium LM25. The initial temperature of the casting is 650°C and the die 200°C. The heat capacity and conductivity values are functions of temperature and the radii rates (eutectic and dendritic) are functions of undercooling and are shown in Figure 15.

The casting and mould are modelled using 4,917 ten-node elements and 10,422 nodes. The meshes of the mould and casting are shown in Figure 16. The process of

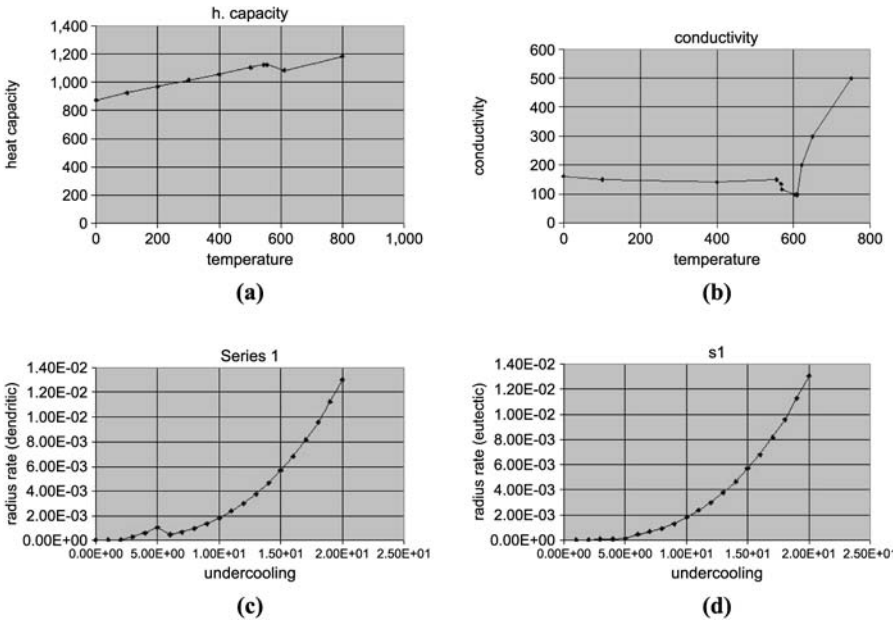

Figure 15.
Material properties (a, b, d, c): heat capacity and conductivity vs temperature, eutectic and dendritic radius rates vs undercooling

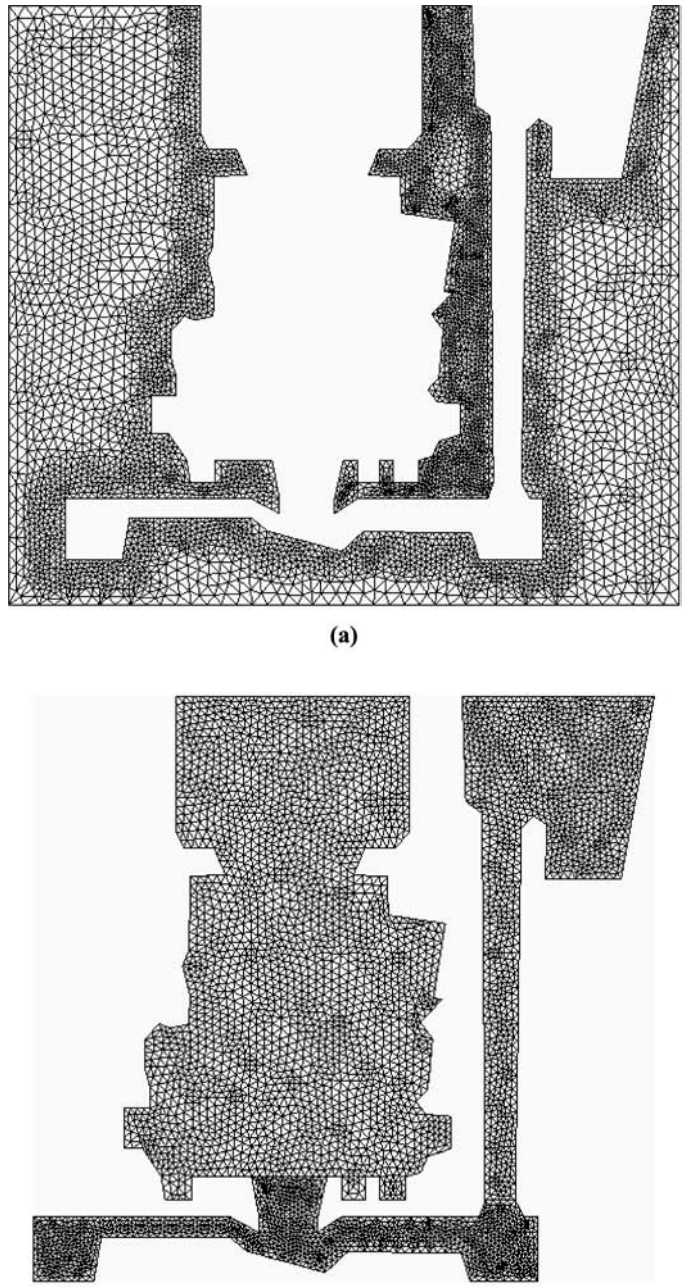

Figure 16.
Finite element mesh of the die (a) and the cast (b)

mould filling is followed until the cavity is almost filled (95 s) and is shown in Figure 17 (distribution of the pseudo-concentration function). The left, lower branch of the mould is still unfilled at this time. The temperature distribution and velocity field are shown in Figure 18.

The distribution of the main microstructural variables, namely, distributions of the liquidus, dendritic and eutectic fractions are shown in Figure 19. It may be seen that the dendritic fraction is concentrated in the thinner part of the section (inlet and lower part of the valve) while the eutectic fraction is concentrated in the main body of the component.

5.2 Thermal stress (microstructural solidification)

An example of the solidification and thermal stress analysis of a wheel is presented. The die and cast are discretized with 25,108 isoparametric bricks and 22,909 nodes. The discretization scheme is shown in Figure 20. The material of the casting is aluminium LM25 and the material of the mould is steel H13.

The temperature distribution is shown in Figure 21. The distribution of the main microstructural solidification model internal variables (i.e. liquidus, dendritic fraction, eutectic fraction) is shown in Figure 22(a)-(c). The distribution of the eutectic and dendritic fractions is similar and almost uniform. The Mises stress distribution is shown in Figure 22(d).

The application of the microstructural model should allow a better prediction of the thermal stress distribution. The solidification already takes place in the filling phase of the process. However, this problem is highlighted in the paper and will be a topic for future research.

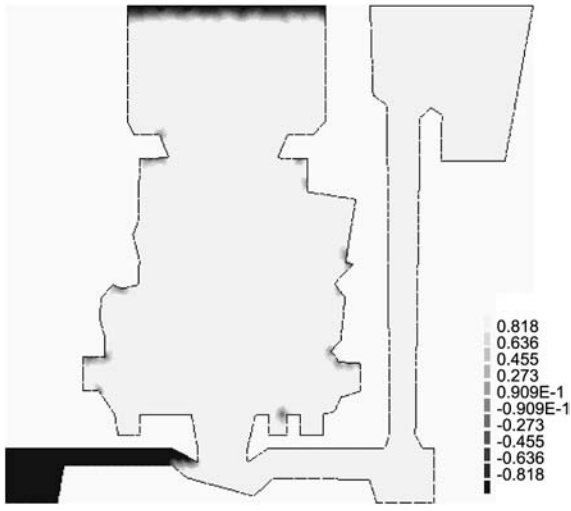

Figure 17.
Pseudo-concentration function distribution, 95 s of the process

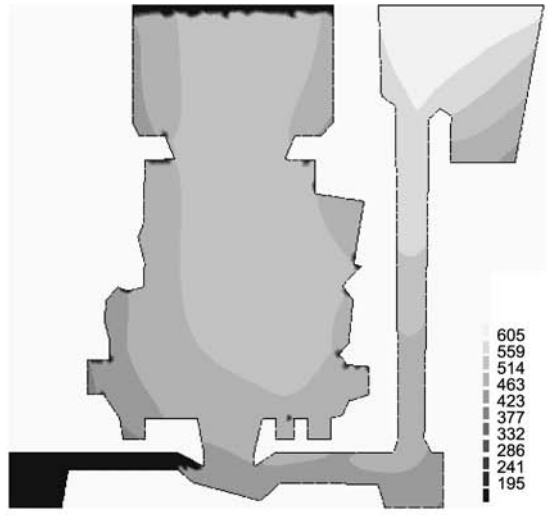

(a)

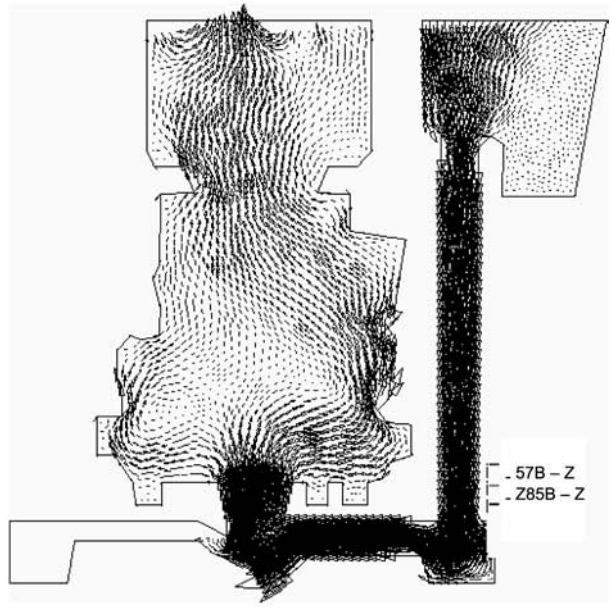

(b)

Figure 18.
Temperature distribution (a), velocity field (b), 95 s

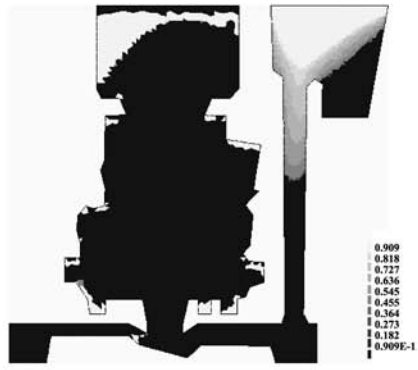

(a)

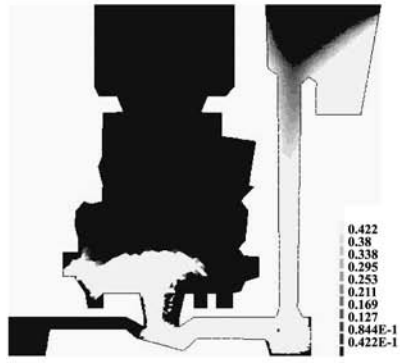

(b)

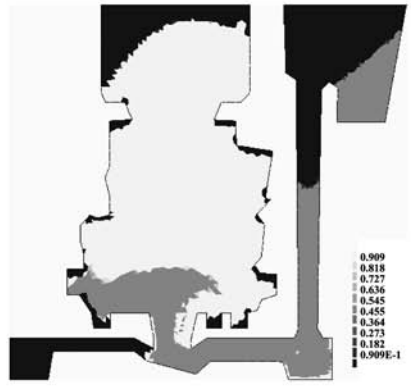

(c)

Figure 19.
Liquidus distribution (a), dendritic fraction distribution (b), eutectic fraction (c)

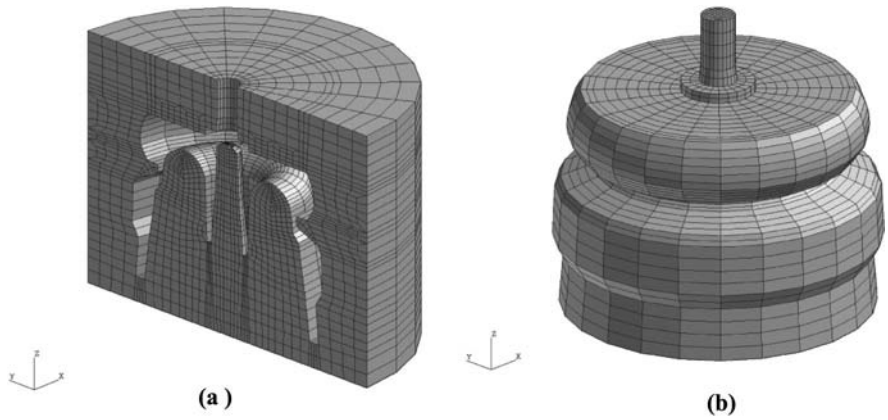

Figure 20.
Wheel, finite element mesh of die (a) and cast (b)

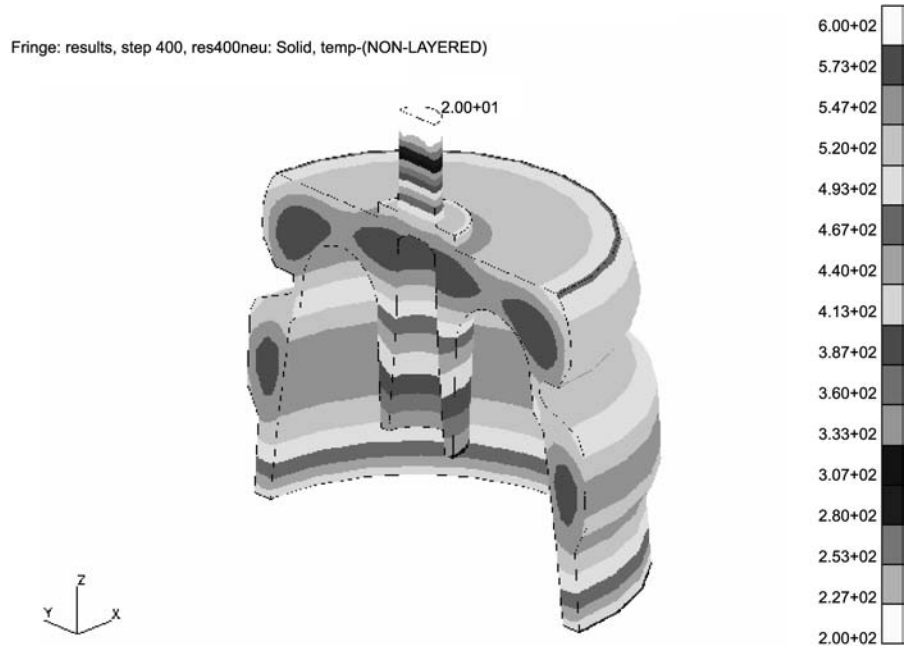

Figure 21.
Temperature distribution in the cast at time 26 s

6. Closure

A mathematical model of the squeeze casting process has been presented. The effectiveness of the developed FE programs has been demonstrated by means of various numerical examples. It may be seen that the model is capable of analysing the complex phenomena of filling, solidification and stress development during the squeeze forming process.

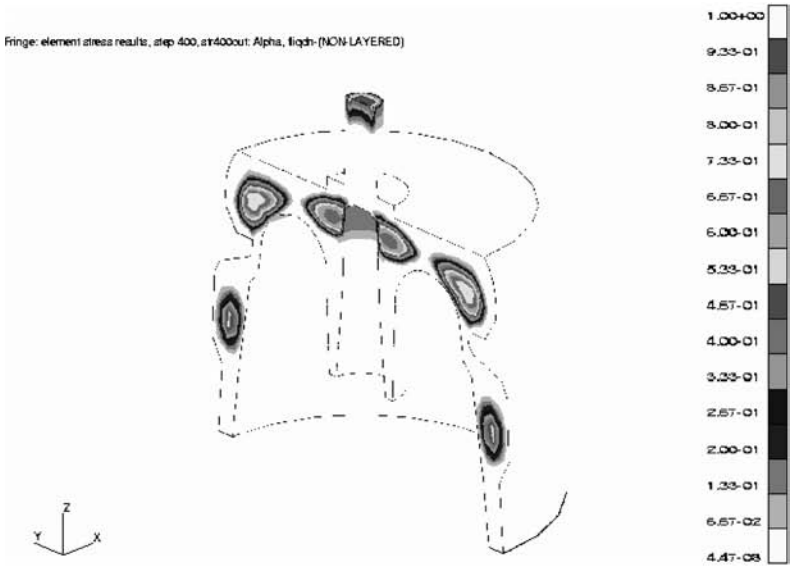

(a)

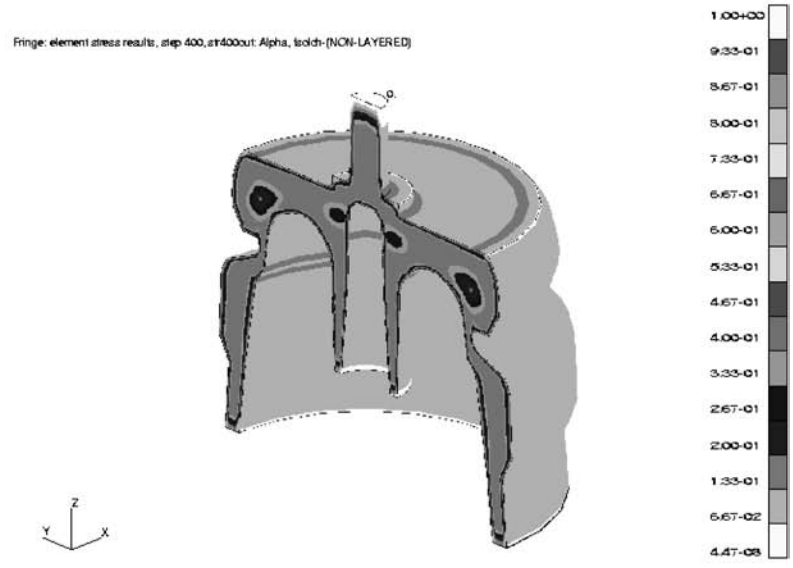

(b)

Figure 22.
Distribution of liquidus (a), dendritic fraction (b), eutectic fraction (c) and Mises stresses at time 26 s

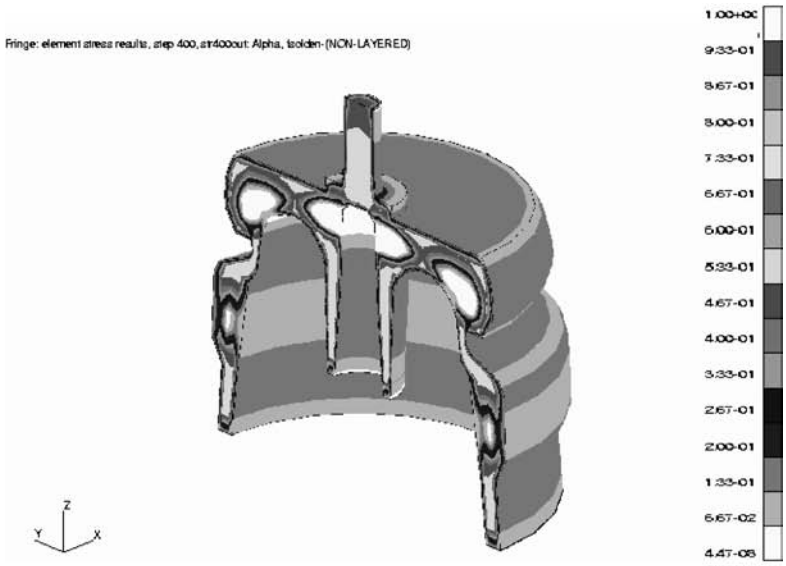
Fringe: element stress results, step 400, str400out: Alpha, isolden-(NON-LAYERED)
1.00+00
9.33-01
8.67-01
8.00-01
7.33-01
6.67-01
6.00-01
5.33-01
4.67-01
4.00-01
3.33-01
2.67-01
2.00-01
1.33-01
6.67-02
4.47-08
Z
Y
X

(c)

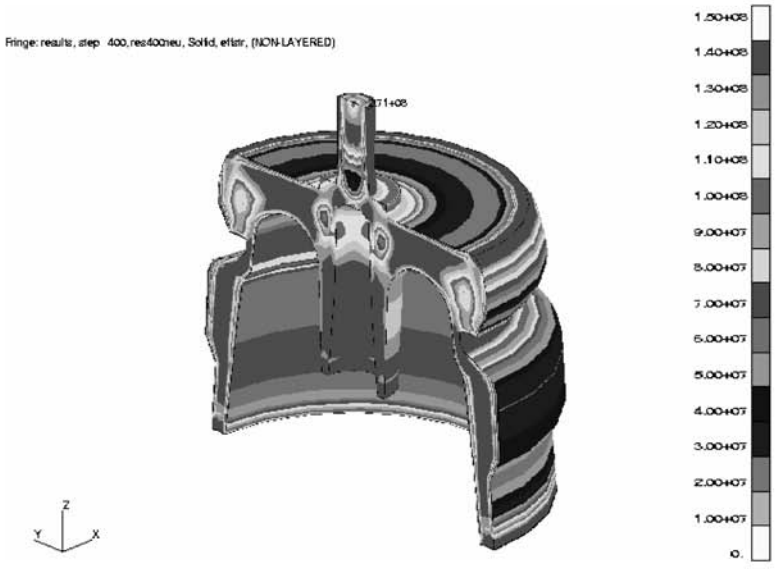
Fringe: results, step 400, res400neu, Solid, eflstr, (NON-LAYERED)
1.50+08
1.40+08
1.30+08
1.20+08
1.10+08
1.00+08
9.00+07
8.00+07
7.00+07
6.00+07
5.00+07
4.00+07
3.00+07
2.00+07
1.00+07
0.
Z
Y
X

(d)

Figure 22.

References

Bathe, K.J. (1996), *Finite Element Procedures*, Prentice-Hall, Englewood Cliffs, NJ.

Braess, H. and Wriggers, P. (2000), "Arbitrary Lagrangian-Eulerian finite element analysis of free surface flow", *Computer Methods in Applied Mechanics and Engineering*, Vol. 190 Nos 1/2, pp. 95-109.

Celentano, D. (1994), "Un modelo termomechanico para problemas de solidification de metales", tesis doctoral, Universidad Politecnica de Catalunya, Barcelona.

Celentano, D.J. (2002), "A thermomechanical model with microstructure evolution for aluminium alloy casting processes", *International Journal of Plasticity*, Vol. 18 No. 10, pp. 1291-335.

Crisfield, M.A. (1991), *Non-Linear Finite Element Analysis of Solids and Structures*, Wiley, New York, NY.

Donea, A. and Huerta, J. (2003), *Finite Element Methods for Flow Problems*, Wiley, New York, NY.

Felippa, C.A. and Park, K.C. (1980), "Staggered transient analysis procedures for coupled dynamic systems", *Computer Methods in Applied Mechanics and Engineering*, Vol. 26 No. 1, pp. 61-112.

Gethin, D.T., Lewis, R.W. and Tadayon, M.R. (1992), "A finite element approach for modelling metal flow and pressurised solidification in the squeeze casting process", *International Journal for Numerical Methods in Engineering*, Vol. 35 No. 4, pp. 939-50.

Ghomashchi, M.R. and Vikhrov, A. (2000), "Squeeze casting: an overview", *Journal of Materials Processing Technology*, Vol. 101 Nos 1/3, pp. 1-9.

Hirt, C.W. and Cook, J.L. (1970), "A Lagrangian method for calculating the dynamics of an incompressible fluid with free surface", *Journal of Computational Physics*, Vol. 5 No. 1, pp. 103-24.

Hirt, C.W. and Nichols, B.D. (1981), "Volume of fluid (VOF) method for the dynamics of free surface boundaries", *Journal of Computational Physics*, Vol. 39 No. 1, pp. 210-25.

Kleiber, M. (1993), "Computational coupled non-associative thermo-plasticity", *Computer Methods in Applied Mechanics and Engineering*, Vol. 90 Nos 1/3, pp. 943-67.

Lewis, R.W. (1996), *MERLIN-An Integrated Finite Element Package for Casting Simulation*, University of Wales, Swansea.

Lewis, R.W. and Ransing, R.S. (1998), "A correlation to describe interfacial heat transfer during solidification simulation and its use in the optimal feeding design of castings", *Metallarurgical and Material Transactions B*, Vol. 29 No. 2, pp. 437-48.

Lewis, R.W. and Ransing, R.S. (2000), "The optimal design of interfacial heat transfer coefficients via a thermal stress model", *Finite Elements Analysis and Design*, Vol. 34 No. 2, pp. 193-209.

Lewis, R.W. and Ravindran, K. (2000), "Finite element simulation of metal casting", *International Journal for Numerical Methods in Engineering*, Vol. 47 Nos 1/3, pp. 29-59.

Lewis, R.W., Morgan, K., Thomas, H.R. and Seetharamu, K.N. (1996), *The Finite Element Method in Heat Transfer Analysis*, Wiley, New York, NY.

Lewis, R.W., Morgan, K. and Zienkiewicz, O.C. (1978), "An improved algorithm for heat conduction problems with phase change", *International Journal for Numerical Methods in Engineering*, Vol. 12 No. 7, pp. 1191-5.

Lewis, R.W., Navti, S.E. and Taylor, C. (1997), "A mixed Lagrangian-Eulerian approach to modelling fluid flow during mould filling", *International Journal for Numerical Methods in Fluids*, Vol. 25 No. 8, pp. 931-52.

Lewis, R.W., Usmani, A.S. and Cross, J.T. (1995), "Efficient mould filling simulation in castings by an explicit finite element method", *International Journal for Numerical Methods in Fluids*, Vol. 20 No. 6, pp. 493-506.

Malcevic, I. and Ghattas, O. (2002), "Dynamic-mesh finite element method for Lagrangian computational fluid dynamics", *Finite Elements in Analysis and Design*, Vol. 38 No. 10, pp. 965-82.

Malvern, L.E. (1969), *Introduction to the Mechanics of Continuous Medium*, Prentice-Hall, Englewood Cliffs, NJ.

Owen, D.R.J. and Hinton, E. (1980), *Finite Elements in Plasticity*, Pineridge Press, Swansea.

Perzyna, P. (1971), "Thermodynamic theory of viscoplasticity", *Advances in Applied Mechanics*, Academic Press, New York, NY, Vol. 11, pp. 313-54.

Ravindran, K. and Lewis, R.W. (1998), "Finite element modelling of solidification effects in mould filling", *Finite Elements in Analysis and Design*, Vol. 31 No. 2, pp. 99-116.

Sluzalec, A. (1992), *Introduction to Nonlinear Thermomechanics*, Springer Verlag, Berlin.

Souli, M. and Zolesio, J.P. (2001), "Arbitrary Lagrangian-Eulerian and free surface methods in fluid mechanics", *Computer Methods in Applied Mechanics and Engineering*, Vol. 191 Nos 3/5, pp. 451-66.

Taylor, C. and Hughes, T.G. (1981), *Finite Element Programming of the Navier Stokes Equations*, Pineridge, Swansea.

Thevoz, Ph., Desbiolles, J. and Rappaz, M. (1989), "Modelling of equiaxed microstructure formation in casting", *Metallurgical Transactions A*, Vol. 20A No. 10, pp. 311-22.

Usmani, A.S., Cross, J.T. and Lewis, R.W. (1992), "A finite element model for the simulation of mould filling in metal casting and the associated heat transfer", *International Journal for Numerical Methods in Engineering*, Vol. 35 No. 4, pp. 787-806.

Usmani, A.S., Cross, J.T. and Lewis, R.W. (1993), "The analysis of mould filling in castings using the finite element method", *Journal of Materials Processing Technology*, Vol. 38 Nos 1/2, pp. 291-302.

Vaz, M. and Owen, D.R.J. (1996), *Thermo-Mechanical Coupling: Models, Strategies and Application*, CR/945/96, University of Wales, Swansea.

Zienkiewicz, O.C. and Taylor, R.L. (2000), *The Finite Element Method*, 5th ed., Butterworth-Heinemann, Oxford.

Corresponding author
Eligiusz W. Postek can be contacted at: e.w.postek@swansea.ac.uk